Doctoral Dissertation

Visualization of quorum sensing metabolites in bacteria biofilms using mass spectrometry imaging

Rattanaburi Pitchapa

June 2023

Biotechnology Global Human Resource Development Program,
Division of Advanced Science and Biotechnology,
Graduate School of Engineering,
Osaka University

Table of Contents

List of Abbreviations

(in alphabetical order)

AHLs: *N*-acyl homoserine lactone

AIs: Autoinducers

AIPs: Autoinducing peptides

DESI: Desorption Electrospray Ionization

DHB: 2,5-dihydroxybenzoic acid

HCD: high cell density

ITO: Indium Tin Oxide

LC: Liquid Chromatography

LCD: low cell density

LC-MS: Liquid Chromatography coupled Mass Spectrometry

MALDI: Matrix-Assisted Laser Desorption/Ionization

MALDI-IT-TOF: MALDI coupled with Ion Trap and Time-of-Flight Mass Spectrometer

MALDI-MSI: Matrix-Assisted Laser Desorption/Ionization Mass Spectrometry Imaging

MS: Mass Spectrometry

MS/MS: tandem mass spectrometry

MSI: Mass Spectrometry Imaging

m/z: mass-to-charge ratio

QS: quorum sensing

ROI: region of interest

SIMS: Secondary Ion Mass Spectrometry

Chapter 1
General Introduction

Biofilm formation is an important adaptation and survival strategy commonly employed by bacteria (Flemming and Wuertz 2019). Bacteria in the biofilm are protected from adverse environmental factors and immune responses (Hall-Stoodley et al. 2004). Biofilms can be composed of multiple species that interact with each other. Notably, single-specie biofilms have subpopulations with different expression patterns and metabolites (López and Kolter 2010; van Gestel et al. 2015). Quorum sensing (QS) is the regulation of gene expression in response to fluctuations in cell-population density. QS system is controlled by chemical signals molecules that regulate traits including bioluminescence, virulence, symbiosis, different forms of motility, biofilm formation, production of antibiotics and toxins, conjugation, and metal chelation (Venturi 2006). Biofilm formation depends on the surface it is on and requires research into its chemical composition, temporal regulation and spatial distribution. Understanding the role of quorum sensing in biofilm formation is important for addressing microbial biofilm growth issues. *Pseudomonas putida* (*P. putida*) is a well-known bacterium that forms biofilms, which are involved in bacterial rhizosphere competence to promote plant growth (Steidle et al. 2002; Purtschert-Montenegro et al. 2022). *P. putida* in the form of biofilms were potentially used as the biosurfactant in the bioremediation of heavy metals (Choi et al. 2003; Lin et al. 2021). In addition, *P. putida* was also used as the biotic-biofilm treatment in oil and sewage pipelines to mediate the corrosion-inhibitive and biopassivating effects of steel (Suma et al. 2019). However, knowledge of the *P. putida* QS system and its role in biofilm formation is limited, even though mass spectrometry imaging (MSI) has recently been used as a promising technique to image quinolones, surfactants, and antibiotics in biofilms (Lanni et al. 2014; Dunham et al. 2017). In this thesis, the sample preparation and cultivation method for widespread mass spectrometry-based chemical imaging of agar-based biofilms were then developed.

1.1 Biofilm

1.1.1 General information

Biofilms are multicellular microbial communities that represent the most common lifestyle of many microorganisms. The unique architecture of biofilms allows these microbial structures to persist in a wide range of niches (Davey et al. 2000). A biofilm can originate from a single microbial species or from numerous and diverse microorganisms, potentially encompassing multiple domains of life (Irie et al. 2008). Importantly, even in biofilms containing a single species, individual cells within different regions of the structure exhibit distinct genetic programs and secreted metabolites due to different subpopulations of cells (Boles et al. 2004).

Biofilm formation is a process, in which microorganism cells transform from planktonic to a sessile mode of growth. The process of biofilm formation occurs through a series of events leading to adaptation under diverse nutritional and environmental conditions (Hentzer et al. 2005). This is a multi-step process in which the microorganisms undergo certain changes after adhering to a surface as shown in Figure 1.1. Microorganisms that form biofilms are shown to elicit specific mechanisms. Biofilm formation has the following important steps (i) planktonic cells attach to the surface (ii) cells proliferate to form microcolonies (iii) three-dimensional structure of mature biofilm are formed and exopolymeric substances are produced (iv) cells disperse back to a planktonic lifestyle and release back to the environment.

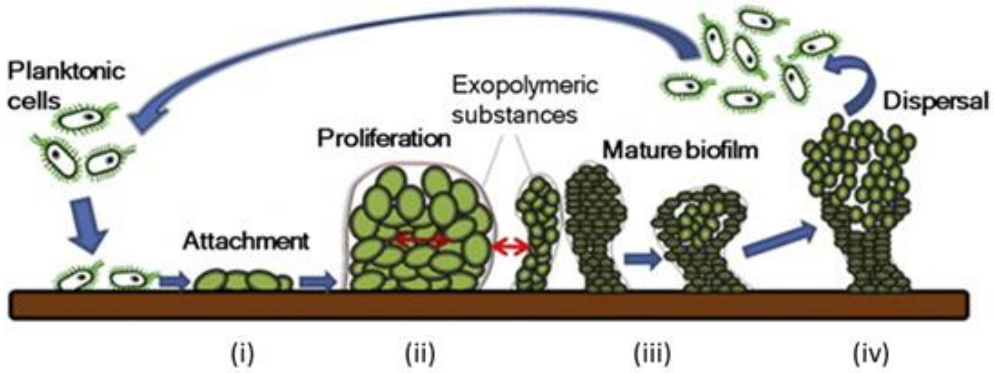

Figure 1.1 The steps of biofilm formation including (i) attachment (ii) cells proliferation (iii) maturation (iv) cells dispersion

One of the key elements in the establishment and maintenance of the biofilm structure and properties is the extracellular matrix. In most biofilms, the microorganisms account for less than 10% of the dry mass, whereas the matrix can account for over 90%. The matrix consists of a conglomeration of different types of biopolymers known as exopolymeric substances (EPS) that forms the three-dimensional architecture of the biofilm and is responsible for adhesion to surfaces and for cohesion in the biofilm. EPS are composed of polysaccharides, proteins, and extracellular DNA that encourage immobilizing biofilm cells and keeping them in close proximity, thus allowing for intense interactions, including cell–cell communication, and the formation of synergistic microconsortia (Flemming et al. 2010; Di Martino 2018).

Recent evidences indicate that many bacterial species use quorum sensing to coordinate the disassembly of the biofilm community. Quorum sensing is a cell-to-cell communication mechanism involving chemical signal molecules that increase in concentration as a function of cell density (Solano et al. 2014). Therefore, understanding quorum sensing systems related to biofilm architecture is important as many problems are raised from the bacterial biofilm. Because quorum sensing regulatory networks are usually very complicated and may include several genes whose products affect biofilm development at different stages, it is not always easy to understand how the activation of quorum sensing finally triggers biofilm dispersion. Consequently, a new approach such as mass spectrometry imaging (MSI) is becoming a powerful tool to study the correlation between quorum-sensing metabolites and biofilm formation by directly visualizing the metabolites inside the biofilm without the prior knowledge of the target genes involved.

1.1.2 *Pseudomonas putida* biofilm

Gram-negative bacteria of the genus *Pseudomonas* are well known for their biofilm formation ability. Among them, *Pseudomonas aeruginosa* is the most popular model organism for studying biofilm formation and is the most studied microorganism with regard to quorum sensing (Tuon et al. 2022). As this species is an opportunistic pathogen that causes several infections in humans (Nathwani et al. 2014; Turkina et al. 2019) become increasingly difficult due to its remarkable capacity to resist antibiotics (Pang et al. 2019), many studies have focused on infections caused by biofilms arising from them (Skariyachan et al. 2018; Ma et al. 2022; Li et al. 2023). Since *P. aeruginosa* is a Biosafety

Level 2 (BSL-2) pathogen, BSL-2 laboratories with the equipment to control the moderate risk of contamination towards worker and environment is required. On the contrary, *Pseudomonas putida*, is also a well-studied biofilm-forming bacterium with the BLS-1 level. This specie is involved in bacterial rhizosphere competence to promote plant growth (Steidle et al. 2001; Steidle et al. 2002; Molina-Santiago et al. 2019). It has been reported that that the plant root colonizer *P. putida* strain IsoF is able to kill a wide range of soil and plant-associated Gram-negative bacteria with the aid of a type IVB secretion system (T4BSS) that delivers a toxic effector into bacterial competitors in a contact-dependent manner (Purtschert-Montenegro et al. 2022). Moreover, *P. putida* biofilms were potentially used as the biosurfactant in the bioremediation of assimilate benzene, toluene and ethylbenzene using the toluene degradation pathway, and can also utilize p-cymene via *p*-cumate using the *p*-cymene and *p*-cumate catabolic pathways (Choi et al. 2003; Weimer et al. 2020). *P. putida* CZ1 planktonic cells and its biofilms in LB medium were investigated for resistance against 12 kinds of metals (Lin et al.2021). In addition, *P. putida* was also used as the biotic-biofilm treatment in oil and sewage pipelines to mediate the corrosion-inhibitive and biopassivating effects of steel (Suma et al. 2019). This ubiquity is traced to its remarkably versatile metabolism, adapted to withstand physicochemical stress, and the capacity to thrive in harsh environments. Owing to these characteristics, there is a growing interest in this microbe for industrial use, and the corresponding research has made rapid progress in recent years. However, the process of *P. putida* biofilm formation is still poorly understood due to the lack of knowledge of the quorum sensing system in these biofilms.

Previous studies have shown that *P. putida* QS systems seems rely on *N*-acyl homoserine lactone (AHLs) signal molecules to express certain phenotypic traits in a cell density dependent manner (Elasri et al. 2001; Steidle et al. 2002). It has been reported that the tomato rhizosphere isolate *P. putida* IsoF produces a wide spectrum of AHLs (Steidle et al. 2001) including 3-oxo-dodecanoyl-homoserine lactone (3-oxo-C12-HSL), 3-oxo-decanoyl-homoserine lactone (3-oxo-C10-HSL) and as minor products, 3-oxo-octanoyl-homoserine lactone (3-oxo-C8-HSL), and 3-oxo-hexanoyl-homoserine lactone (3-oxo-C6-HSL). Whereas some strains of *P. putida* could produce only a few AHLs, for example, strain WCS358 has been shown to produce only 3-oxo-C12-HSL (Bertani et al.

2004) and strain T2-2 produces both C8-HSL and C12-HSL (Chen et al. 2013). In contrast of other *Pseudomonas*, *P. putida* KT2440 was reported to produce the AHLs signal molecules directed by the AHL synthase PpuI, which the regulatory protein PpuR binds to the QS signal molecules and controls the ppuI expression in a positive feedback loop (Fernández et al. 2011). This system is different to the LasI/LasR system of *P. aeruginosa* and others strains of *P. putida*. It appears that the QS metabolites that *P. putida* could produce are strain-specific. Therefore, advances in analytical techniques are necessary to characterize *P. putida*'s quorum sensing system in order to expand our knowledge of their biofilm formation and its impact.

1.2 Bacterial Quorum Sensing systems and their role in biofilm formation

1.2.1 General concept

Quorum sensing (QS) is a bacterial cell-to-cell communication process that involves the production, detection, and response to extracellular signaling molecules called autoinducers (AIs). AIs accumulate in the environment as the bacterial population density increases, and bacteria monitor this information to track changes in their cell numbers and collectively alter gene expression. QS controls genes that direct activities that are beneficial when performed by groups of bacteria acting in synchrony. Processes controlled by QS include bioluminescence, sporulation, competence, antibiotic production, biofilm formation, and virulence factor secretion (Novick et al. 2008; Ng et al. 2009).

Despite differences in regulatory components and molecular mechanisms, all known QS systems depend on three basic principles. First, the members of the community produce AIs, which are the signaling molecules. At low cell density (LCD), AIs diffuse away, and, therefore, are present at concentrations below the threshold required for detection. At high cell density (HCD), the cumulative production of AIs leads to a locally high concentration, enabling detection and response (Kaplan et al. 1985). Second, AIs are detected by receptors that exist in the cytoplasm or in the membrane. Third, in addition to activating the expression of genes necessary for cooperative behaviors, the detection of AIs results in the activation of AI production (Novick et al. 1995; Seed et al. 1995). This feed-forward autoinduction loop presumably promotes synchrony in the population.

Gram-positive and Gram-negative bacteria use different types of QS systems (Fig. 1 shows the four paradigmatic QS wiring diagrams). Gram-positive bacteria use peptides, called autoinducing peptides (AIPs), as signaling molecules. Once produced in the cell, AIPs are processed and secreted. When the extracellular concentration of the AIP is high, which occurs at HCD, it binds to a cognate membrane-bound two-component histidine kinase receptor. Generally, binding activates the receptor's kinase activity, it autophosphorylates, and passes phosphate to a cognate cytoplasmic response regulator. The phosphorylated response regulator activates the transcription of the genes in the QS regulon (Fig. 1.2A). In some cases of Gram-positive bacterial QS, AIPs are transported back into the cell cytoplasm where they interact with transcription factors to modulate the transcription factor's activity and modulate gene expression changes (Fig. 1.2B).

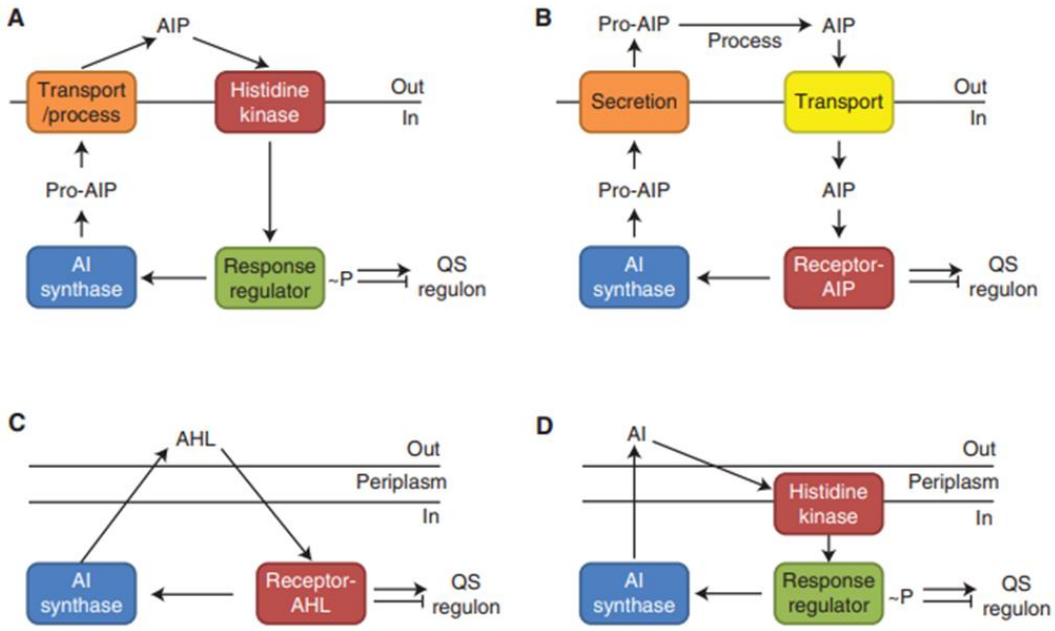

Figure 1.2 Bacterial QS. AIP-QS in Gram-positive bacteria by (A) two-component signaling, or (B) an AIP-binding transcription factor. Small molecule QS in Gram-negative bacteria (C) a LuxI/LuxR-type system, or (D) two-component signaling

Gram-negative bacteria communicate using small molecules as AIs. These are either AHLs or other molecules whose production depends on *S*-adenosylmethionine (SAM) as a substrate (Wei et al. 2011). AIs are produced in the cell and freely diffuse

across the inner and outer membranes. When the concentration of AIs is sufficiently high, which occurs at HCD, they bind cytoplasmic receptors that are transcription factors. The AI-bound receptors regulate expression of the genes in the QS regulon (Fig. 1.2C). In some cases of Gram-negative bacterial QS, AIs are detected by two-component histidine kinase receptors that function analogously to those described in the preceding paragraph for Gram-positive QS bacteria (Fig. 1.2D).

1.2.2 *N*-Acyl-homoserine lactone quorum sensing system

The *N*-Acyl-homoserine lactone (AHLs) quorum sensing system includes specialized metabolites (quorum sensors, virulence factors, and natural products), which are key components that utilize in a signaling pathway in Figure 1.3 to control metabolite production where the transcriptional factor pair RhlI/RhlR is subordinate to the LasI/LasR pair (Pearson et al. 1999). LasI produces *N*-3-oxo-dodecanoyl-L-homoserine lactone (3-oxo-C12-HSL), whereas RhlI produces *N*-butanoyl-L-homoserine lactone (C4-HSL). These homoserine lactones bind to the transcriptional activators LasR and RhlR, respectively, and activate target promoters. Both *las* and *rhl* have been implicated in regulating the production of a signaling metabolite in a group of *Pseudomonas* quinolones signal (Heeb et al. 2011). The homoserine lactones and quinolones have been shown to regulate the expression of genes required for specialized metabolite production, including those for the siderophores pyochelin and pyoverdine, as well as the phenazines, and rhamnolipid molecular families.

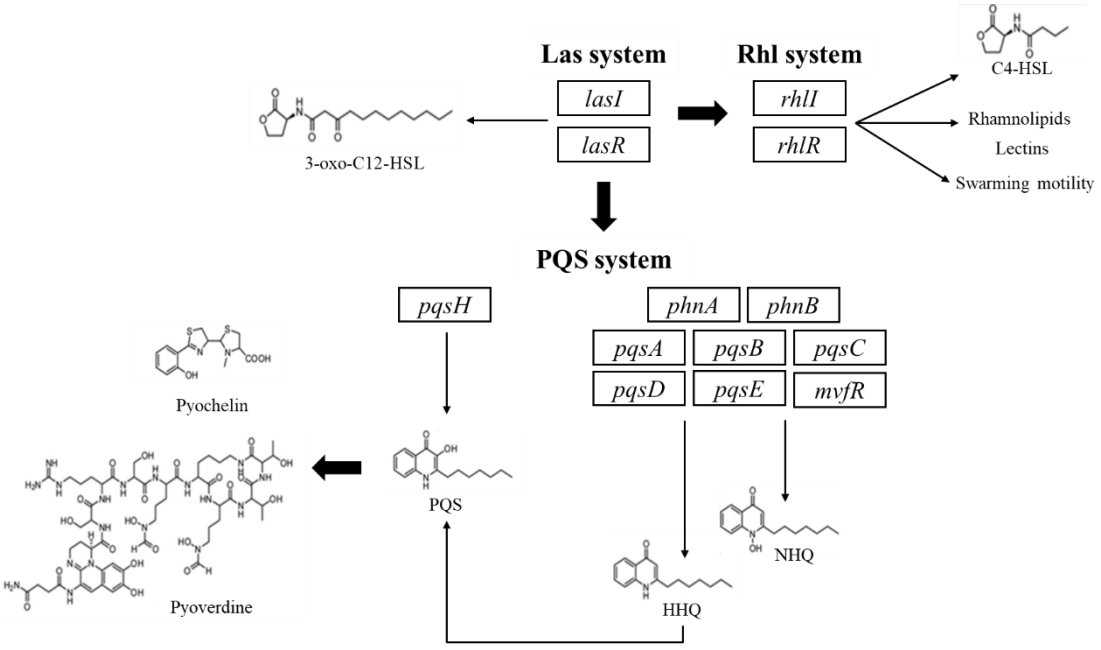

Figure 1.3 AHLs signaling system to control specialized metabolite production.

1.3 Mass spectrometry imaging

1.3.1 General concept

Mass spectrometry imaging (MSI) is a technique to visualize the spatial distribution of analytes on a sample cross-section based on its mass-to-charge ratio (*m/z*) value. In principle, this technology does not require labeling, is able to monitor multiple analytes simultaneously, semi-quantitative, and relatively fast (Canela et al. 2016). Because of these advantages, MSI proves to be a very attractive method to visualize analytes on many kinds of samples, including human and animal tissues, plants, and even food materials (Ikuta et al. 2022; Kokesch-Himmelreich et al. 2022; Takeo et al. 2021).

The basic principle of MSI is the collection of a series of mass spectra from rastering a specified area of a tissue sample. From each acquisition point, a whole mass spectrum is generated. The data matrix will consist of the ion, its intensity, and its x-y coordinate on the sample. From this data, it is possible to visualize the ion intensity distribution and correlate it with the sample's form and structure.

Several ion sources are available for MSI analysis. The most popular ones include matrix-assisted laser desorption/ionization (MALDI), desorption electrospray ionization (DESI), and secondary ion mass spectrometry (SIMS); each of them with its own strength

and weaknesses. As such, the selection of technique depends on the objective of the study (Vickerman 2011; Shimma 2022).

1.3.2 Matrix-assisted laser desorption/ionization mass spectrometry imaging

Matrix-assisted laser desorption/ionization mass spectrometry imaging (MALDI-MSI) is one of the most widely used technique for MSI. The technique is commonly applied for a wide range of samples, and high-spatial resolution imaging (compared to DESI) is possible by modifying the laser diameter and matrix application. Figure 1.4 shows the workflow of imaging by MALDI-MSI.

Sample sectioning is one of the most important steps in MSI analysis. Sample sectioning is usually done by cryosectioning, as the below-freezing temperature maintains the morphology of most samples during sectioning. For small samples with diameters less than 1 cm, it is common to first embed it into an embedding material before the sectioning step. The thickness of the sections used for MSI analysis ranges from 8 µm to 100 µm. Thinner sections are usually preferred since it is known to increase ion detectability (Sugiura et al. 2006). However, acquiring thin sections depends on the sample's sturdiness. The sections are then mounted onto a conductive glass slide coated with Indium Tin Oxide (ITO) by thawing (Dong et al. 2016).

The sectioned sample is applied by matrix before laser irradiation. The function of the matrix is to assist desorption/ionization of target metabolites as well as reducing fragmentation that may occur from high laser energy. Consequently, matrix compounds are usually has aromatic rings in their structure, which are known to be able to absorb energy from UV lights (Leopold et al. 2018). Many matrix substances are available commercially, and each matrix has different efficiency in different analysis modes and for different groups of metabolites. The purpose of matrix application in MALDI-MSI is to uniformly coat the matrix on the surface of sample in order to reduce the possibility of concentrated spots that may produce higher ion intensity and hinder correct interpretation of the ion distribution. This is usually achieved by spraying dissolved matrix in a solvent to the surface of the sample. Spraying can be done manually by using an airbrush or an automatic sprayer. Another method is by sublimating the matrix powder onto the sample surface (Hankin et al. 2007). This method usually needs a special instrument to control the temperature and pressure condition of the sublimation instrument.

After matrix application, samples are subjected to analyze using a MALDI-MS instrument that is already modified to suit MSI analysis. This modification includes the software used or the ability to take pictures of the sample within the instrument. It is important to be able to determine the area of analysis that correlates with the shape or area of interest of samples. The laser will irradiate the samples on predetermined points with a fixed distance between each point. The samples irradiated will produce a plume of ions, which will be transported to the mass spectrometer.

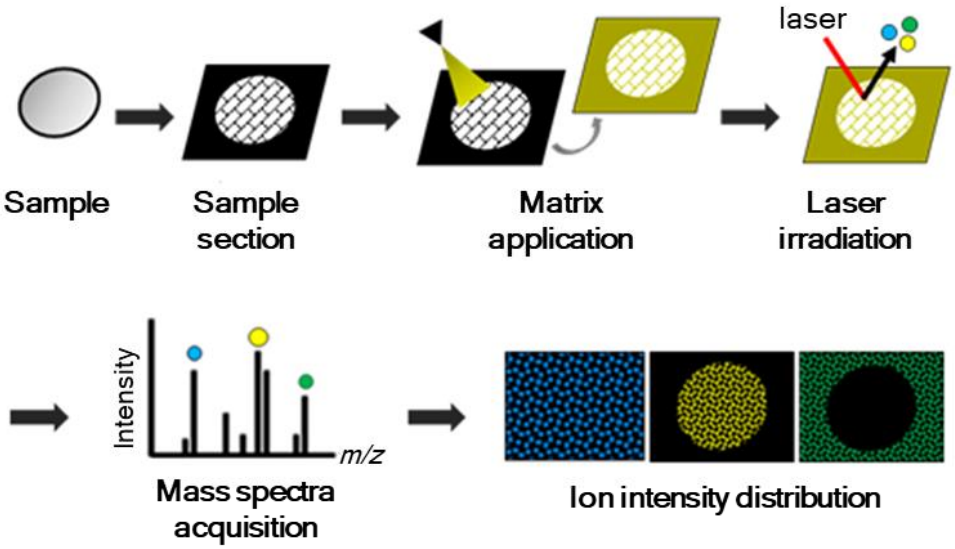

Figure 1.4 MALDI-MSI workflow including sample preparation, matrix application, and visualization

1.3.3 Application of MALDI-MSI for biofilm research

Representing approximately half of all microbial MSI publications, MALDI offers the most comprehensive coverage of molecular species. Lipids, peptides, and proteins are all accessible with the proper matrix selection, and the technique commonly achieves a spatial resolution of better than 100 μm for microbial samples. Important applications of MALDI-MSI in microbiology include the visualization of chemical interactions between different species of *P. aeruginosa* and *Staphylococcus aureus* (Frydenlund et al. 2016), characterization of surfactants and peptides produced by different strains of *Bacillus subtilis* (Si et al. 2016), imaging of nutritionally dependent *P. aeruginosa* proteins produced in a heterogeneous drip-flow reactor (Wakeman et al. 2016), and

characterization of the chemical response of *P. aeruginosa* to the addition of the antibiotic azithromycin (Phelan et al. 2015). These studies and many others illustrate the potential of MALDI-MSI in both fundamental biological discovery and medical research.

Recently, MALDI-MSI visualization of *P. putida* biofilms has been reported (Li et al. 2018). With this method, drip flow biofilms cultivation, vacuum desiccator, and sublimation with 2,5-dihydroxybenzoic acid (DHB), lipids and oligosaccharides distribution across a *P. putida* biofilm was visualized. However, quorum sensing molecules were not successfully observed in this work. Therefore, new method is required for visualization of quorum sensing metabolites and their distributions in *P. putida* biofilm using MALDI-MSI.

1.4 Objective of this study

As previously stated, quorum sensing metabolites regulate the bacterial biofilm formation involving in various traits of bacteria such as virulence, symbiosis, and metal chelation. Even though, biofilms generated by single-specie bacteria, they have subpopulations with different expression patterns and metabolites. However, detailed information on the heterogeneity of QS metabolites in biofilms remains largely unknown, especially in the case of *P. putida* biofilms, due to the lack of a suitable analytical approach and versatile biofilm cultivating method. MALDI-MSI was recently attempted to map the metabolites in *P. putida* biofilms. However, no studies on the visualization of QS compounds produced by this species of biofilm have been successful.

The aim of this study is to establish a protocol for the widespread use of mass spectrometry imaging for the analysis of agar-based biofilms. The approach will involve the following steps:

1. Development of a biofilm formation method suitable for MALDI-MSI analysis, including biofilm cultivation and sample preparation.
2. Optimization of the MALDI-MSI analysis method, through the selection of an appropriate matrix application condition.
3. Validation of the biofilm formation method through the use of MALDI-MSI to visualize the distribution of AHL metabolites.

1.5 Thesis outline

This thesis includes five chapters that describe the steps in the study of the visualization of quorum sensing metabolites in bacteria biofilms using mass spectrometry imaging. The first chapter provides a general introduction to biofilms, the *P. putida* biofilm, which was chosen as the model organism in this study, bacterial QS systems and their role in biofilm formation, with a particular emphasis on the AHLs-QS system. In chapter two, the agar-based biofilm method was developed and applied to *P. putida* biofilms. In chapter three, the time course analysis was done to determine the correlation between the production of AHLs metabolites and biofilm development in *P. putida*. In Chapter 4, genome sequencing of *P. putida* 6157 was performed to confirm the results detected by MALDI-MSI, which indicate the existence of the AHLs system in *P. putida* 6157. Finally, the conclusion obtained from this study were summarized, and future perspectives were proposed in chapter five.

Chapter 2

Development of Agar-based biofilm method for MALDI-MSI

2.1 Introduction

In the field of biofilm research, Matrix-Assisted Laser Desorption/Ionization Mass Spectrometry Imaging (MALDI-MSI) has recently been used as a promising technique to image quinolones, surfactants, and antibiotics (Phelan et al. 2015; Frydenlund Michelsen et al. 2016; Si et al. 2016). MALDI-MSI could provide the composition, form, and spatial information of the metabolites inside biofilms. In contrast to other existing chemical imaging technologies, MSI does not require any molecular labeling mechanism and can be applied to analyze used to identify multiple molecular species in one experiment (Caprioli et al. 1997). This technique employs a matrix homogeneously applied to the sectioned samples to encourage the desorption/ionization of compounds and reduce fragmentation during laser irradiation. Mass spectral data is collected and the resulting data can be collated to generate the ion images based on intensity. Ion images reveal the spatial distributions of metabolites within the sample (Norris et al. 2013; Moore et al. 2014).

Although MSI is frequently employed in the study of microbial biofilms, several challenges linked to the hydrated, absorbent, deformable, soft, and non-uniform nature of the biofilm surface remain in obtaining reliable ion images (Yang et al. 2009). MALDI-MSI with the drip flow reactor method for biofilm cultivation has been applied to visualize metabolites in *P. putida* biofilms. Drip flow reactor was used as the conventional method for MALDI-MSI analysis of bacteria biofilms. The *P. putida* strain F1 (ATCC 700007) was cultivated statically at 30°C for 6 h in a logarithmic growth phase with a drip angle of 0°. After 6 h, the drip angle was increased to 5°, and a continuous flow of nutrients was supplied at 50 mL/h via peristaltic pump through a glass flow break to establish single-strain biofilms on the stainless steel surfaces. Biofilm samples were then subjected for pretreatment via vacuum desiccation and mass imaging. This conventional method allowed the distribution of lipids and oligosaccharides to be observed across *P. putida* biofilms. However, this prior use of the drip flow reactor in the visualization of *P. putida* biofilm metabolites was also deemed unsuccessful in detecting the QS metabolites (Li et al. 2018). The previous report also indicates a dramatic decrease in the intensity of

QS compounds after 48 hours of inoculation (Baig et al. 2015), whereas the drip flow reactor method requires at least 72 hours for biofilm cultivation. In addition, this drip flow reactor technique requires special equipment for biofilm cultivation: a drip flow biofilm reactor and stainless steel coupons or glass slides that fit MALDI adapter plates. As a result of these technological problems, the biofilm formation method for MALDI-MSI, which provides a robust biofilm within 48 hours, is required to map the spatial distribution of QS metabolites in *P. putida* biofilms. Therefore, this chapter aims to develop a novel cultivation and sample preparation workflow for widely targeted MS-based chemical imaging of agar-based biofilms. *P. putida* 6157 was selected as the model organism in this work. This strain is BSL-1, which was reported as a plant co-colonization bacterial biofilm with *B. subtilis* 3610 to promote plant growth during the rhizosphere competence. *P. putida* 6157 was found to secrete a compound, 2,4-diacetylphloroglucinol, that inhibits biofilm gene expression and cell differentiation of *B. subtilis* 3610 during the co-colonization (Powers et al., 2013). The mutants of all the *B. subtilis* 3610 EPS were cultivated together with *P. putida* 6157 on LB agar to investigate their respective contribution at 48, 72, and 96 hours. The absence of EPS resulted in increased fluidity and loss of structure of the *B. subtilis* biofilms. However, the information on biofilm development, the QS system, and the heterogeneity of metabolites across the 6157 strain is still understudied. Consequently, this information is needed in order to understand the mechanism driving biofilm formation of this strain, which might expand the information on the interactions between these plant-beneficial bacteria.

2.2 Experimental

2.2.1 Bacterial Strain and Reagents

P. putida 6157 (Japan Collection of Microorganisms, Japan) was used for biofilm cultivation. All chemicals used for the LB media were purchased from Becton Dickinson (Sparks, MD, USA). The MALDI matrices, 2,5-dihydroxybenzoic acid (DHB), and α-cyano-4-hydroxycinnamic acid (CHCA), were purchased from Sigma-Aldrich (St. Louis, MO, USA). Methanol was purchased from WAKO Pure Chemical Industries (Osaka, Japan). Ultrapure water was obtained using a Genpure UV-TOC xCAD Plus (Thermo Fisher Scientific, Waltham, MS, USA).

2.2.2 Agar-based biofilm formation

P. putida 6157 was first cultured at 26°C for 15 h to stationary phase (OD_{600}=0.05, ~1.0×10^6 CFU/mL) in LB liquid medium from a single colony (Fig. S1). The culture (1 μL) was then inoculated on thin layer LB agar medium (10 mL in a standard 10-cm petri dish, and typically contains 2% w/v agar) which contained the indium-tin-oxide (ITO)-coated glass slide for MALDI-MSI (100 Ω/m^2 without anti-peeling coating, Matsunami Glass, Osaka, Japan). The petri dishes are either sealed with parafilm to minimize dehydration of the thin agar during incubation. The biofilm was then cultivated in static condition at 26°C for 48 h in order to obtain the mature stage of biofilms.

2.2.3 MALDI matrix application

The MALDI matrices DHB and CHCA were applied to the biofilm surfaces via spot test. Selected MALDI matrix powder was then applied to the biofilm samples with spraying using manual airbrush application and sublimation. The thickness of the matrix was optimized at 0.5 μm for coverage homogeneity and sensitivity. For sublimation, matrix was heated at 180 °C and deposited onto the surface of biofilms in an iMLayer (Shimadzu, Kyoto, Japan).

2.2.4 MALDI-MSI analysis

MSI was performed using an iMScope TRIO instrument (Shimadzu, Kyoto, Japan). Both optical images under microscopic conditions and ion distribution images could be obtained using the same instrument under atmospheric pressure. An Nd:YAG laser (λ = 355 nm, 1 kHz) was used as the MALDI laser source, and laser irradiation was repeated 100 times on each pixel with a laser power of 45.0 (in arbitrary units). Mass spectra were acquired in the positive-ion detection mode with the *m/z* range of 100–1000 for visualization of QS metabolites in *P. putida* 6157 biofilms. After obtaining the mass spectra, the peak intensity maps were reconstructed using Imaging MS Solution software (Shimadzu, Kyoto, Japan).

2.3 Results and Discussion

As the utilization of conventional methods for inducing biofilm formation failed to provide a comprehensive depiction of the distribution of quorum-sensing metabolites within *P. putida* biofilms, the objective of this step is to devise a method for culturing biofilms that can be subjected to MALDI-MSI analysis.

2.3.1 Agar-Based Biofilms for MALDI-MSI

The workflow used for the construction, cultivation, and characterization of the agar-based biofilms for MALDI-MSI is shown in Figure 2.1. The MALDI-MSI analysis workflow starts with the cultivation of *P. putida* directly on an ITO-coated glass slide embedded in a thin layer of agar medium prior to inoculation with *P. putida*. In case of *P. putida* biofilm cultivation, a medium that used in this study is LB medium (10 g/L tryptone, 5 g/L yeast extract, 5 g/L sodium chloride, and 1.5% agar). The agar is 1 to 1.5 mm thick, equivalent to 10 to 11 mL medium in a standard 10-cm petri dish, and typically contains 2% agar. The ITO-coated glass slide was deposited in the center of Petri dishes prior to the pouring of the LB agar and *P. putida* inoculation which are either sealed with parafilm to minimize dehydration of the thin agar during incubation, or incubated for various times at 26 °C (Fig. 2.1A, B). After the incubation, biofilm sample with the height less than 1.0 mm was obtained. The biofilm and surrounding agar attached to the glass slide were then directly subjected for MSI analysis (Fig. 2.1C, E). Lastly, MALDI-MSI and metabolite annotation were performed (Figure 1D, E).

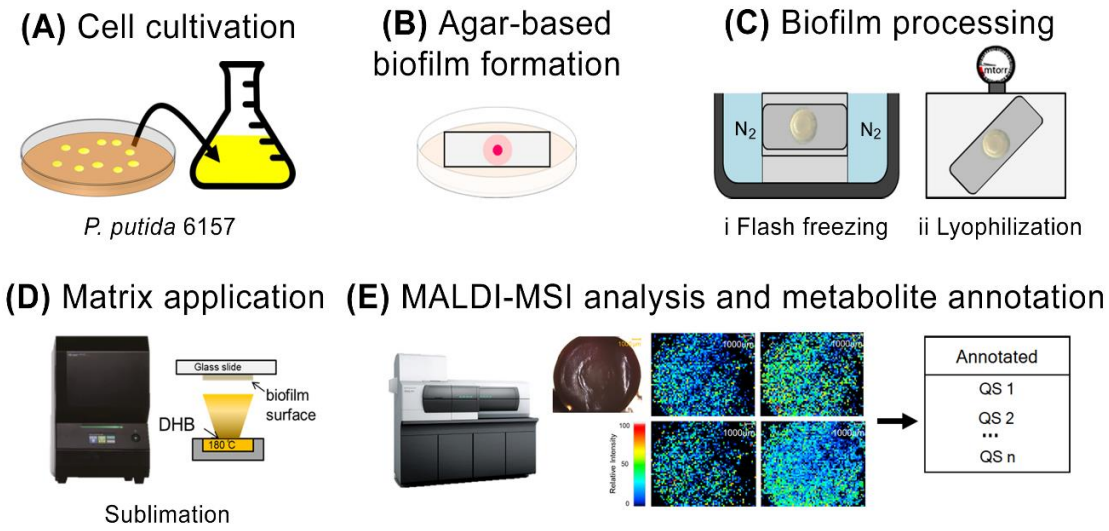

Figure 2.1 Workflow for cultivation and preservation of agar-based biofilms. (A) Cell cultivation. (B) Adherence and formation of bacterial biofilms onto the ITO glass slide surface. (C) Pretreatment of biofilms by flash-freezing and lyophilization. (D) Matrix sublimation and (E) MALDI-MSI analysis and metabolite annotation to distinguish ions specific to different biofilm regions

However, the biofilm sample showed insufficient adherence to the target surface. Substantial peeling and flaking of the biofilm were observed during the matrix application, which involved a change from normal to high vacuum pressure inside the instrument (Fig 2.2B). The term flaking is used to describe air bubbles, fissures, and partial or complete detachment of the dehydrated biofilm sample from the ITO glass slide. Consequently, the biofilm samples were subjected to specific biofilm processing which involving reducing the pressure gap to address this adherence issue and minimize flaking.

Two approaches of biofilm processing were selected, low vacuum container and flash-freezing in liquid nitrogen prior to lyophilization, respectively. Time for dehydration was optimized in both of methods (Fig. S4). The methods were evaluated by the morphology of biofilm, number of peak of detection, and peak intensity of quorum sensing candidate at *m/z* 325.07. The effect of DHB matrix thickness and sublimated time towards peak intensity of *m/z* 325.07 and the percentage compared to highest matrix peak; *m/z* 273.04 was determined and presented in Figure S2.

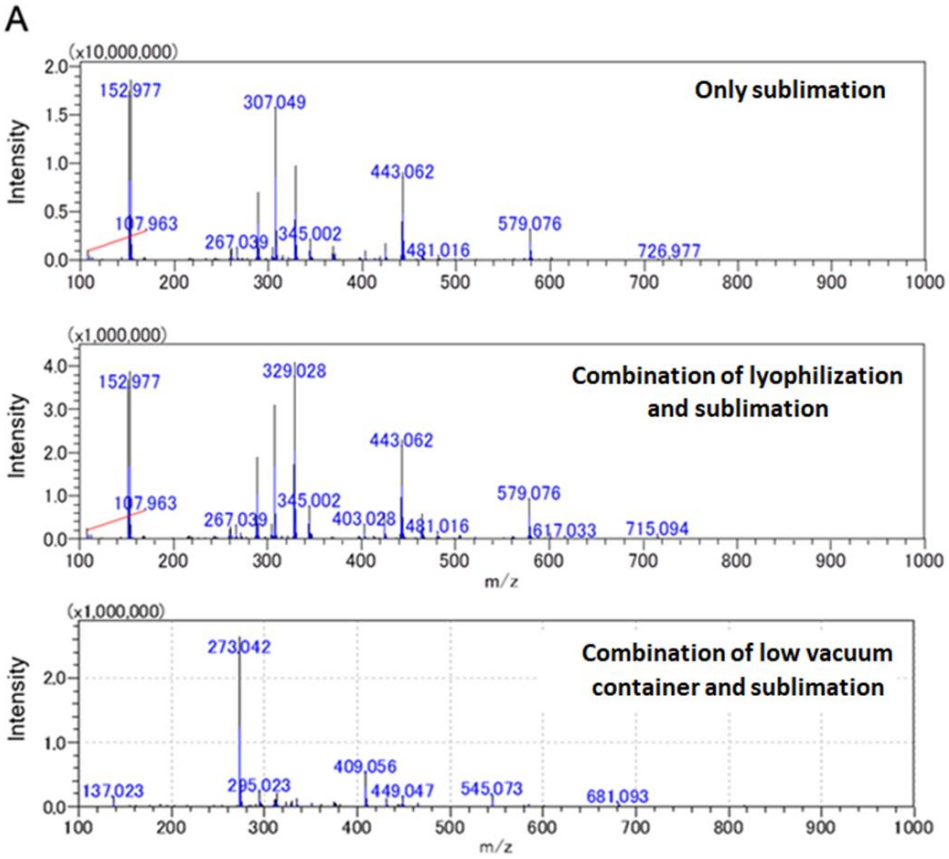

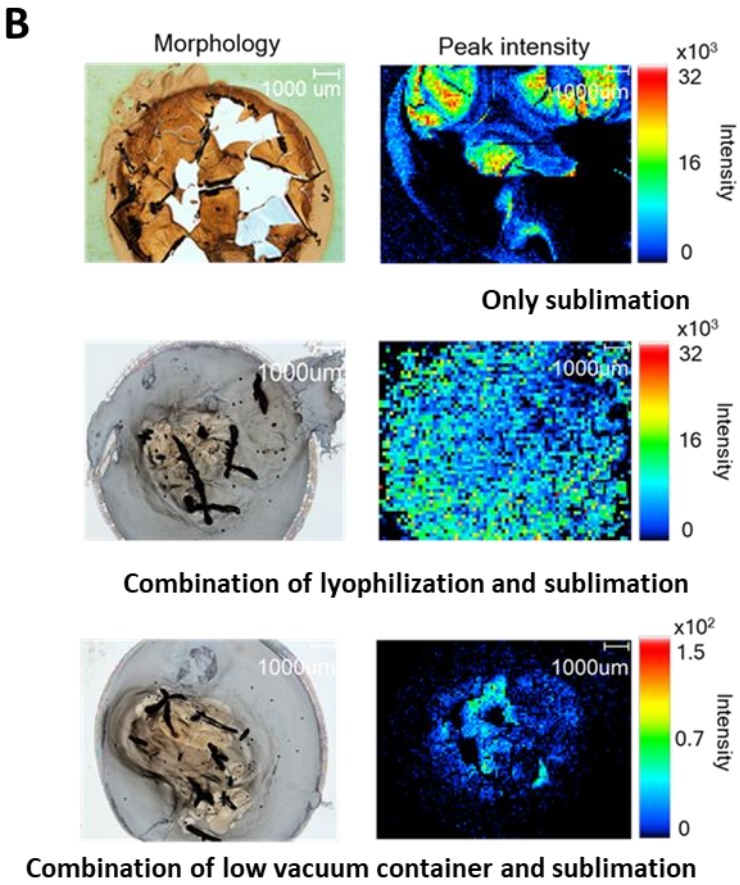

Figure 2.2 Comparison between biofilm processing methods compared with direct sublimation. The parameters for method evaluation was (A) number of peak detection, (B) biofilm morphology, and intensity of quorum sensing candidate at *m/z* 325.07

The results of the comparison between two methods with a directly sublimation with 0.5 µm thickness of DHB (Fig. S2) as shown in Figure 2.2. For the number of peak detection, lyophilization shows the similar pattern of MS spectra compared with sublimation. In contrast with low vacuum container method, almost detected peak detected are originated from DHB matrix (Fig. 2.2A). However, the peak intensity of lyophilization was 10 times lower than directly sublimation. It has been reported that quorum sensing metabolites are time-sensitive molecules. After 48 hours of biofilm cultivation, the intensity of quorum sensing metabolites in *P. aeruginosa* were dramatically decreased (Baig et al. 2015). Thus, it is possible that the peak intensity during the biofilm processing was affected by the time of dehydration. However, lyophilization could solve flaking problem and provide the best biofilm morphology with

the high peak intensity of quorum sensing candidate compared with others (Fig. 2.2B). Furthermore, the number of detected peaks obtained from the process with and without the biofilm flash-freezing and lyophilization steps was similar (Fig. 2.3A).

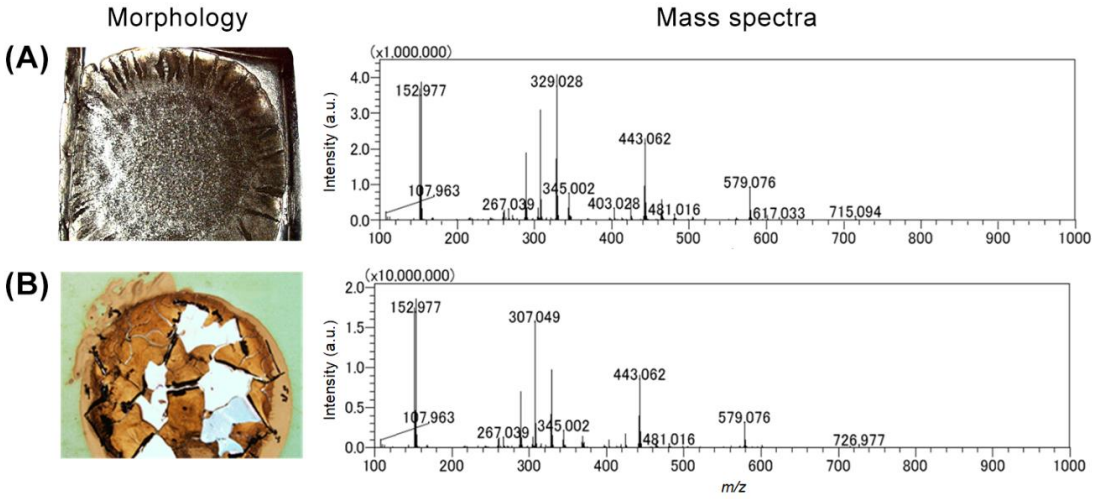

Figure 2.3 Morphology of modified agar-based biofilms and the mass spectra obtained with (A) and without biofilm processing (B)

The methodology of biofilm formation predicated on agar produces static biofilms, affording it a multitude of advantages relative to overflow systems. The static system necessitates no specialized infrastructure, is cost-effective, and straightforward to establish. In many cases, static biofilms are a format amenable to high-throughput screening, thereby facilitating the rapid evaluation of the impact of a mutant library or array of culture conditions on biofilm formation. The workflow of agar-based biofilm formation producing static biofilms in the form of colony biofilms makes it ideal for colony biofilm assays. This technique is optimal for replicating natural biofilms that are not typically immersed in liquid. In addition to MALDI-MSI visualization, the susceptibility of agar-based biofilm samples to antibiotics, ultraviolet radiation, and oxidative or other environmental stresses can also be tested. Thus, the methodology of agar-based biofilm formation and its associated techniques may be utilized to examine the spatially adaptive response of bacterial biofilms under a wide gamut of experimental conditions.

2.3.2 Optimization for MALDI matrix application

Matrix application is a crucial step in MALDI-MSI analysis. An appropriate matrix and application method must be considered in order to achieve a high-quality visual of compound distribution on the sample surface. The optimization for the MALDI matrix application is separated into two steps: optimization of the type of matrix and optimization of the application method.

- Optimization of the type of matrix

Two commonly used MALDI matrices, DHB and CHCA, were tested and spotted onto the surfaces of agar-based biofilm samples prior to MALDI-MSI analysis. The DHB matrix powder provided a more homogeneous matrix crystal and broader coverage of a higher number of detected metabolites (including candidate AHL-QS molecules) with higher ion intensity than the CHCA matrix powder as presented in Figure 2.4.

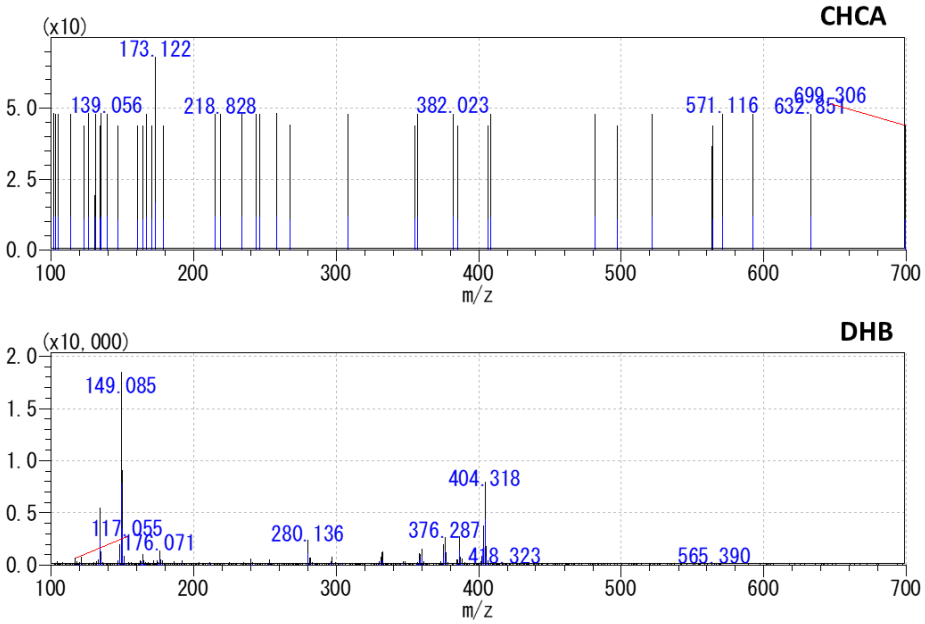

Figure 2.4 Comparison of MS spectra obtained from the spot test between CHCA and DHB matrices

- Optimization of the application method

Two widely used application methods, sublimation and spraying, were compared in this study. Applying matrix through sublimation forms a layer consisting of evenly distributed, tiny matrix crystals (Hankin et al. 2007). The small crystal formation in the

sublimation method is considered beneficial, especially in high-resolution imaging. In the spraying method, spraying matrix solution is done by using an airbrush. The spraying method aids in extracting the analytes from a sample surface and is said to give a high intensity with a good signal-to-noise ratio. The most commonly used matrix in positive mode imaging of molecules, DHB, was used for all methods.

The main purpose of this optimization step was to get a high signal intensity and clear distribution of the quorum-sensing compounds in the *P. putida* 6157 biofilm. The number of peaks detected and the peak intensity of the candidate QS molecule with *m/z* 325.07 was also used for the method evaluation.

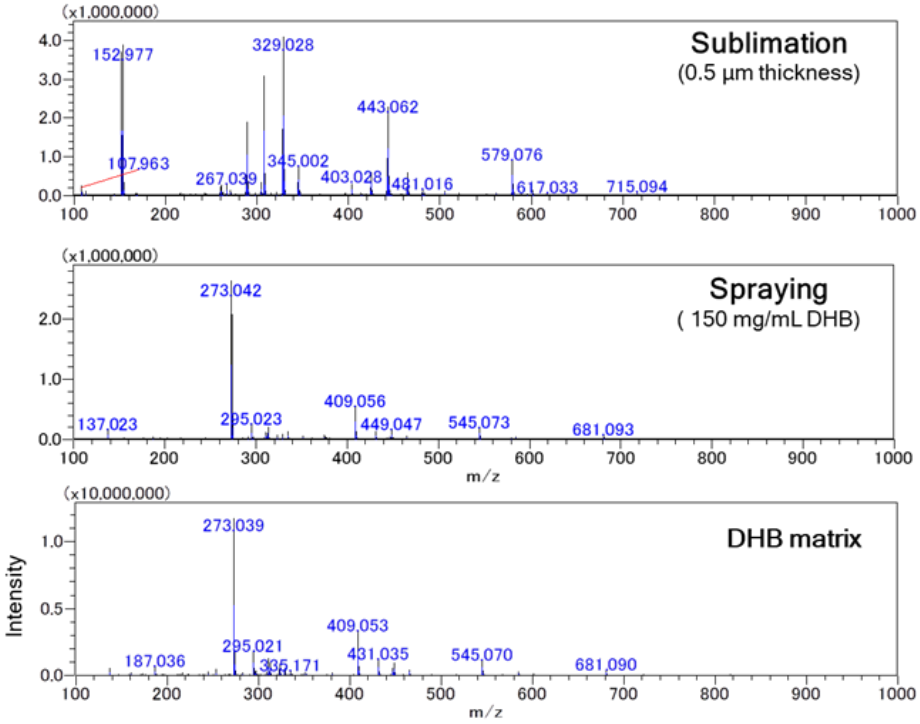

Figure 2.5 MS spectra obtained from two matrix application methods, sublimation and spraying

After biofilm samples were coated with DHB matrix by sublimation or spraying at the optimized concentration 150mg/mL (Fig. S3), the MS spectra were then obtained and compared for method evaluation (Fig. 2.5). Almost all of the detected peaks from the spraying method are derived from the DHB matrix. In contrast, sublimation gives a high number of peak detections, including the candidate peaks of quorum-sensing metabolites.

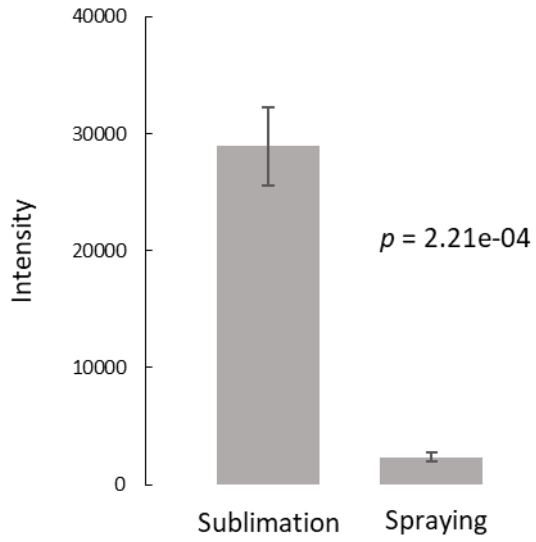

Figure 2.6 Comparison of *m/z* 325.07 intensity between sublimation and spraying. Error bars represent the standard deviation (n = 6), *P*-value based on two-way *t-test* = 2.21e-04

Sublimation produces a better result in peak intensity of the quorum-sensing candidate, which is consistent with the number of peak detection results. The average peak intensity at *m/z* 325.07 obtained from three ROIs of the inner part (the region of inoculation) and three ROIs of the outer part of three biofilm samples were determined and calculated. The yield of the sublimation method was approximately 10 times higher than spraying (Fig. 2.6). As a result, sublimation was chosen as a suitable method for matrix application in order to visualize quorum sensing metabolites in *P. putida* 6157 biofilms.

2.3.3 Visualization of quorum sensing metabolites in *P. putida* biofilms

MALDI-MSI visualization with the developed agar-based biofilm method was conducted to detect quorum sensing metabolites in *P. putida* biofilms. Instead of screening the related genes using conventional methods such as genetic complementation of the mutant gene, transposon mutagenesis, or liquid chromatography mass spectrometry (LC-MS), this study used MALDI-MSI to observe the spatial distribution of AHLs-QS compounds in *P. putida* 6157 biofilms. Due to the limitations of the conventional approaches, such as the complexity of genes controlling biofilm formation and the

extraction process required to remove exopolymeric substances before LC surgery, MALDI-MSI would overcome these problems. By this approach, it is expected that observing AHLs-QS compounds in *P. putida* 6157 directly related to structural differences would be much more efficient.

At 48 hours after incubation, images of candidate metabolites for AHLs-QS were obtained using MALDI-MSI with the agar-based biofilm method across *P. putida* 6157 biofilms as shown in Figure 2.7. Four metabolites that might be including in AHLs-QS system with their spatial distribution were observed from *P. putida* 6157 biofilms with the *m/z* 244.17, *m/z* 260.16, *m/z* 272.21, and *m/z* 325.07 respectively. These results show the robustness of the developed agar-based biofilm workflow since AHLs-QS metabolite were successfully visualized by MALDI-MSI for the first time.

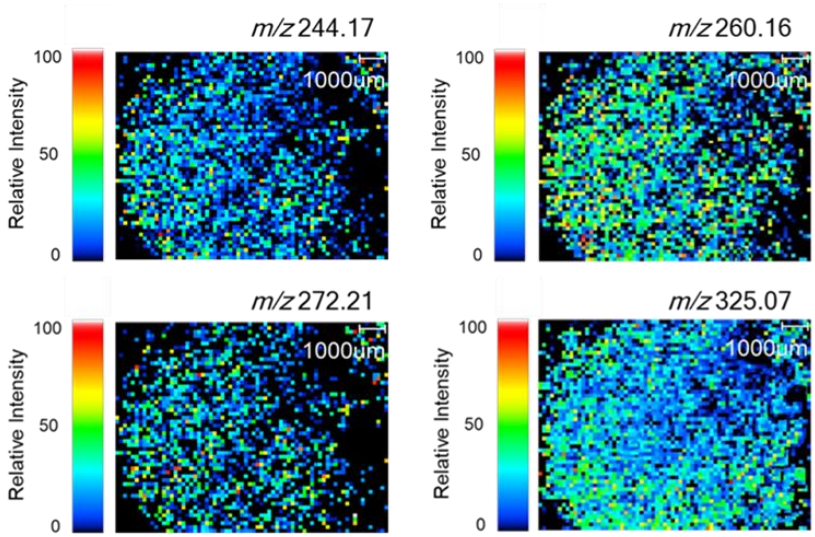

Figure 2.7 Images of the candidate metabolites for AHLs-QS visualized via MALDI-MSI with agar-based biofilm method in *P. putida* 6157 biofilms at 48h

2.4 Conclusion

In this chapter, the agar-based biofilm workflow was the first successful strategy to yield robust and reproducible flat biofilms 48 h after inoculation. The workflow starts with the cultivation of *P. putida* directly on an ITO-coated glass slide embedded in a thin layer of agar medium prior to inoculation with *P. putida*. After incubation for 48 hours reach to the mature stage of biofilm development, the biofilm and surrounding agar

attached to the glass slide were directly used for MSI analysis. However, the biofilm sample showed insufficient adherence to the target surface. Substantial peeling and flaking of the biofilm were observed during the sublimation process, which involved a change from normal to high vacuum pressure inside the instrument. The term flaking is used to describe air bubbles, fissures, and partial or complete detachment of the dehydrated biofilm sample from the ITO glass slide. To address this adherence issue and minimize flaking, the biofilm samples were subjected to specific biofilm processing, including flash-freezing in liquid nitrogen and lyophilization. This step was performed to ensure that good biofilm morphology was preserved during sublimation. For the MALDI matrix application, DHB matrix powder with sublimation was selected as it provided a more homogeneous matrix crystal and broader coverage of a high number of detected metabolites (including AHL-QS molecules). After the DHB matrix was sublimated onto the biofilm surfaces, MALDI-MSI and metabolite annotation were performed. Notably, the utilization of agar-based biofilms in MALDI-MSI enables the first visualization of AHL-QS metabolites and their distributions within *P. putida* biofilm. This method can be used to observe the spatially adaptive response of bacterial biofilms under a wide variety of experimental conditions. The agar-based biofilm approach proposed in this study was used to prepare biofilm samples for MSI because it has a lower risk of contamination. Furthermore, it can be used to study more than one colony per target plate, increasing sample throughput and allowing numerous samples to be processed via a single MALDI-MSI analysis.

Chapter 3

Correlation between the production of AHLs metabolites and biofilm development in *P. putida* 6157

3.1 Introduction

As mentioned the previous chapter, a novel workflow for MALDI-MSI of bacterial biofilms, agar-based biofilm formation method, was developed. It is necessary to elucidate the robustness of this technique. Thus, the experiments in this chapter focusing on the determination of the relationship between the spatial distribution of QS metabolites produced by *P. putida* 6157 and the stage of biofilm formation. This work first performed MS analysis of the biofilm samples incubated at 26 °C for 6, 12, 24, and 48 h after inoculation. The biofilms were grown for 6 and 12 h represented the early stage of the biofilm, whereas those grown for 24 and 48 h showed features of mature biofilms.

The elaboration of complex biofilm communities proceeds through four main stages (Landini et al. 2010; Crouzet et al. 2014; Tolker-Nielsen 2015; Ruhal et al. 2021; Sauer et al. 2022): (i) bacterial attachment to a surface, (ii) microcolony formation, (iii) biofilm maturation, and (iv) detachment (also termed dispersal) of bacteria, which may then colonize new areas.

- Early stages of biofilm development

For the early stages of biofilm development, including stages 1 and 2, cells undergo a reversible attachment phase during which they may leave the substratum. This is followed by irreversible attachment, at which point cells become permanently associated with the surface. Next, cells form clusters or microcolonies and start becoming mature biofilms.

- Biofilm maturation

In the mature stage of biofilm formation, cell residents begin to produce an adhesive matrix that enables cells to stick to one another to form a multilayer biofilm. The matrix, or extrapolymeric substance (EPS), is primarily composed of exopolysaccharide, protein, and DNA. In addition to EPS production, a second transition occurs during biofilm maturation, namely downregulation of flagella synthesis. Flagella synthesis is involved

in swarming motility. Swarming motility is a process by which bacteria can rapidly advance on moist surfaces in a coordinated manner. It requires functional flagella and is coupled to the production of a viscous slime layer. The slime layer is thought to extract water from the agar and keeps the cells in a moist environment. Swarming is a group behavior that requires the cells to reach a certain cell number before the process is initiated. Swarming is widespread in many genera of Gram-negative and Gram-positive flagellated bacteria and is typically assayed on a solidified medium, containing 0.5-2% agar, from which the bacteria are thought to extract water and nutrients (Verstraeten et al. 2008).

- Biofilm detachment

The last step in biofilm development is dispersion. A multilayer biofilm can be viewed as a collection of heterogeneous microenvironments. As such, bacterial residents within the biofilm experience a myriad of different conditions depending on their location. Cells in the interior have reduced access to nutrients and possibly increased exposure to toxic byproducts compared with those positioned at the surface.

3.2 Experimental

3.2.1 Bacterial Strain and Reagents

P. putida 6157 (RIKEN, Japan) was used for biofilm cultivation. All chemicals used for the LB media were purchased from Becton Dickinson (Sparks, MD, USA). The MALDI matrix, DHB, was purchased from Sigma-Aldrich (St. Louis, MO, USA). Methanol was purchased from WAKO Pure Chemical Industries (Osaka, Japan). Ultrapure water was obtained using a Genpure UV-TOC xCAD Plus (Thermo Fisher Scientific, Waltham, MS, USA).

3.2.2 Agar-based biofilm formation

P. putida 6157 was first cultured at 26°C for 15 h to stationary phase. (OD_{600}=0.05, ~1.0×10^6 CFU/mL) in LB liquid medium from a single colony. The culture (1 μL) was then inoculated on thin layer LB agar medium (10 mL in a standard 10-cm petri dish, and typically contains 2% w/v agar) which contained the indium-tin-oxide (ITO)-coated glass slide for MALDI-MSI (100 Ω/m^2 without anti-peeling coating, Matsunami Glass, Osaka, Japan). The petri dishes are either sealed with parafilm to minimize dehydration of the thin agar during incubation. The biofilm was then cultivated in static condition at 26°C.

Agar-based biofilms were sampled at 6, 12, 24, and 48 hours for the time-course analysis to examine the distribution of QS metabolites within biofilms associated with the different stages of biofilm formation.

3.2.3 Matrix application

The DHB matrix was applied to the biofilm surfaces via sublimation. The thickness of the DHB matrix was optimized at 0.5 μm for coverage homogeneity and sensitivity. For sublimation, DHB was heated at 180 °C and deposited onto the surface of biofilms in an iMLayer (Shimadzu, Kyoto, Japan).

3.2.4 MALDI-MSI analysis

MSI was performed using an iMScope TRIO instrument (Shimadzu, Kyoto, Japan). Both optical images under microscopic conditions and ion distribution images could be obtained using the same instrument under atmospheric pressure. An Nd:YAG laser (λ = 355 nm, 1 kHz) was used as the MALDI laser source, and laser irradiation was repeated 100 times on each pixel with a laser power of 45.0 (in arbitrary units). Mass spectra were acquired in the positive-ion detection mode with the *m/z* range of 100–1000 for visualization of QS metabolites in *P. putida* 6157 biofilms. After obtaining the mass spectra, the peak intensity maps were reconstructed using Imaging MS Solution software (Shimadzu, Kyoto, Japan).

3.2.5 Metabolite annotation

Tandem mass spectrometry with a collision energy of 20 or 40 (arbitrary unit in iMScope TRIO) was performed to confirm the selected precursor *m/z* (protonated ion) with predicted QS signals obtained from High Chem Mass Frontier 7.0 (HighChem, Ltd., Brati-slava, Slovak Republic), a software package for the management, evaluation, and interpretation of mass spectra. This software provides several useful tools for processing and organizing mass spectral and chromatographic data.

3.3 Results and discussion

To elucidate the relationship between the spatial distribution of QS metabolites produced by *P. putida* 6157 and the stage of biofilm formation, MSI analysis of the biofilm samples incubated at 26 °C for 6, 12, 24, and 48 h after inoculation was performed. The biofilms were grown for 6 and 12 h represented the early stage of the biofilm, whereas those grown for 24 and 48 h showed features of mature biofilms with the wrinkle of swarming motality (Fig. S5). The QS metabolites detected and mapped on *P. putida* biofilms were not the same at different cultivation times (Figure 3). Two distinct ion groups, including six *m/z*, were observed as QS metabolites in *P. putida* biofilms. The first group included *m/z* 172.09 and *m/z* 298.20, annotated as *N*-butanoyl-L-homoserine lactone (C4-HSL) and *N*-3-oxo-dodecanoyl-L-homoserine lactone (3-oxo-C12-HSL), respectively. These two metabolites were found only in early-stage biofilms and were primarily localized in the region of inoculation. These results suggested that C4-HSL and 3-oxo-C12-HSL might use as precursors to produce other qs metabolites; quinolones and siderophores. The second group included QS metabolites that could only be visualized in the later stages of biofilm development. This group was composed of quinolone metabolites, 2-heptyl-4-quinolone (HHQ), 2-heptyl-3-hydroxy-quinolone (PQS), and 2-nonyl-4-quinolone (NHQ). At 24 hours after inoculation, all quinolones were observed in the outer parts of *P. putida* 6157 biofilms. However, the intensities of quinolones in the inner part of biofilms were higher than the outer part of biofilms. After 48 hours of biofilm formation, quinolones were homogeneously distributed mainly on the outer part of *P. putida* 6157 biofilms. Our experimental *m/z* values of annotated AHLs and quinolones for the protonated molecular ion ($[M + H]^+$) were similar to the data from previous studies, indicating good validation of our analysis method, as presented in Table 1 (Wakeman et al. 2016; Davies et al. 2017). The localization abundance pattern of this second group was more compatible with swarming motility, resulting in the mass movement of cells and, thus, mature biofilm formation. Notably, PQS was the only quinolone observed during the early stages of biofilm formation at 12 h with a homogeneous distribution through the biofilms. Moreover, PQS was clearly observed at the edge of the inner part of *P. putida* 6157. This data suggested that PQS might be the intermediated compound for production of others quinolones. Pyochelin, a siderophore involved in iron chelation, was only visualized in the mature stage of *P. putida* 6157 biofilms, mainly at the biofilm's front

line. In contrast, the repartitioning of the other quinolones was homogenous in the biofilm. These results indicated a clear relationship between the temporal production and spatial distribution of QS metabolites and biofilm development in *P. putida* 6157.

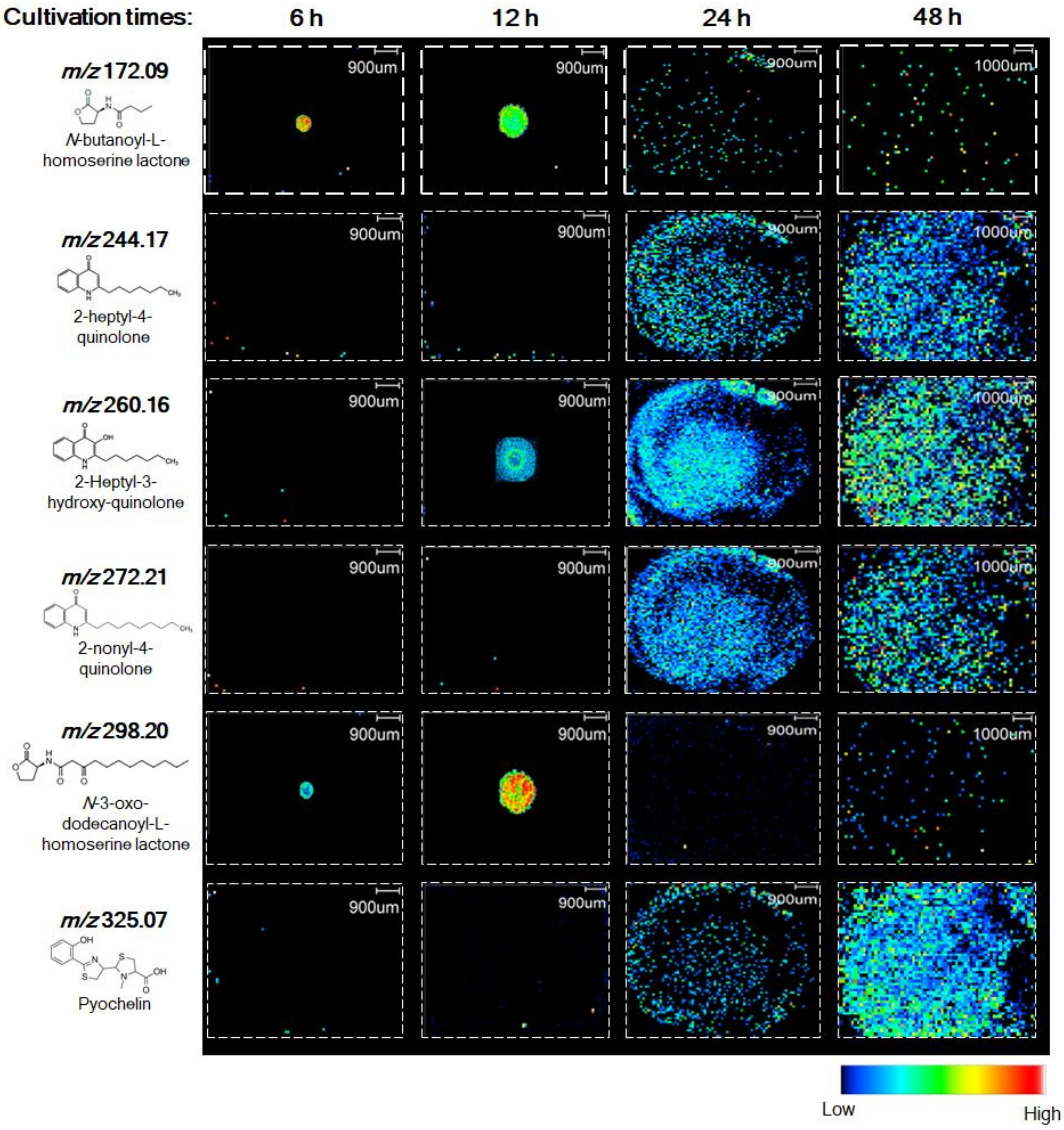

Figure 3.1 MSI images of *N*-acyl-homoserine lactone quorum sensing metabolites including quinolones and siderophore produced by biofilms *P. putida* 6157 grown for 6, 12, 24, and 48 hours.

Compound ID	Molecular Formula	$[M + H]^+$ Theoretical	$[M + H]^+$ Exp.	References
C4-HSL	$C_8H_{13}NO_3$	172.09	172.09	Rodrigues et al. 2022
3-oxo-C12-HSL	$C_{16}H_{27}NO_4$	298.20	298.20	Rodrigues et al. 2022
HHQ	$C_{16}H_{21}NO$	244.17	244.17	Davies et al. 2017
PQS	$C_{16}H_{21}NO_2$	260.17	260.16	Davies et al. 2017
NHQ	$C_{18}H_{25}NO$	272.21	272.21	Davies et al. 2017
Pyochelin	$C_{14}H_{16}N_2O_3S_2$	325.06	325.07	This work

Table 1 *N*-acyl-homoserine lactones and quinolones observed in *P. putida* 6157 biofilms

In addition, EPS compounds including diacylglycerols (DGs) and phosphatidylethanolamine (PE) which were detected via the drip flow reactor method was also visualized by agar-based biofilm method. It has also been report that lipids were proposed to be the primary component of EPS in the pellicle biofilms (biofilms formed at the liquid-air interface of cultures) of *Mycobacterium tuberculosis* (Chakraborty & Kumar 2019). At 48 h after biofilm formation, DG and PE were homogeneously distributed throughout the biofilm with a high intensity compared to QS molecules (Fig S7), which might indicate the mature biofilm features that contain EPS as the barrier of cell population. However, the polysaccharides and proteins were not detected in this work due to the limitation of the imaging mass spectrometry imaging machine, iMScope, which deems to visualize the metabolite with a higher *m/z* than 1500.

The agar-based biofilm workflow was the first successful strategy to yield robust and reproducible static biofilms 48 h after inoculation. These biofilms were used to visualize the heterogeneity of QS metabolites and the correlation between temporal and spatial QS metabolite production and biofilm development in *P. putida*, using MALDI-MSI. Our results showed that C4-HSL and 3-oxo-C12-HSL production was only observed in young biofilms. This agrees with previous work on biofilm formation and QS metabolite production using liquid chromatography coupled with mass spectrometry (LC-MS) (Ca'rcamo-Oyarce et al. 2015). In addition, we demonstrated that the production and distribution of AHL-QS metabolites are correlated with biofilm development as the mass movement for the formation of mature biofilm structures. In this study, quinolones and pyochelin distribution were visualized for the first time in *P. putida*, and the results demonstrated that these metabolites were only observed in mature biofilms.

3.4 Conclusion

In this chapter, a time-course analysis of MALDI-MSI was conducted on biofilm samples incubated at 26 °C for 6, 12, 24, and 48 hours post-inoculation. This examination aimed to shed light on the correlation between the spatial distribution of QS metabolites produced by *P. putida* 6157 and the progression of biofilm formation. Biofilms grown for 6 and 12 hours signified the nascent stage of the biofilm, while those grown for 24 and 48 hours displayed characteristics of mature biofilms. The findings revealed that the QS metabolites detected in *P. putida* biofilms varied over the course of cultivation. Two prominent ion groups, comprised of six *m/z*, were recognized as QS metabolites. The first group, consisting of *N*-butanoyl-L-homoserine lactone (C4-HSL) and *N*-3-oxo-dodecanoyl-L-homoserine lactone (3-oxo-C12-HSL), was present exclusively in early-stage biofilms and concentrated around the point of inoculation. The second group, comprised of quinolone metabolites such as 2-heptyl-4-quinolone (HHQ), 2-heptyl-3-hydroxy-quinolone (PQS), and 2-nonyl-4-quinolone (NHQ), was observable only in mature biofilms and uniformly distributed across the surface of *P. putida* 6157 biofilms. The even distribution of this group suggests swarming motility, resulting in a massive movement of cells and, thus, mature biofilm formation. Notably, PQS was the sole quinolone identified in the early stages of biofilm formation at 12 hours. Pyochelin, a siderophore involved in iron sequestration, was present only in mature *P. putida* 6157 biofilms and primarily located at the forefront. In contrast, the distribution of the other quinolones was uniform throughout the biofilm. These results highlight a distinct association between the production and spatial distribution of QS metabolites with the advancement of biofilm development in *P. putida* 6157. Moreover, it indicates the robustness of the agar-based biofilm workflow towards MALDI-MSI visualization of bacterial biofilms.

Chapter 4

Analysis of the genes involved in the production of AHLs-QS in the genome of *Pseudomonas putida* 6157

4.1 Introduction

The most important concern is the evidence of the presence of quorum sensing system in *P. putida* 6157. Previous studies have shown that *P. putida* QS systems seems rely on *N*-acyl homoserine lactone (AHL) signal molecules to express certain phenotypic traits in a cell density dependent manner (Steidle et al. 2002). It has been reported that the tomato rhizosphere isolate *P. putida* IsoF produces a wide spectrum of AHLs (Steidle et al. 2001) including 3-oxo-dodecanoyl-homoserine lactone (3-oxo-C12-HSL), 3-oxo-decanoyl-homoserine lactone (3-oxo-C10-HSL) and as minor products, 3-oxo-octanoyl-homoserine lactone (3-oxo-C8-HSL), and 3-oxo-hexanoyl-homoserine lactone (3-oxo-C6-HSL). In *P. putida* IsoF, the production of AHL signal molecules is directed by the AHL synthase PpuI, whereas the regulatory protein PpuR binds to the AHL signal molecules and controls the ppuI expression in a positive feedback loop. This system is very similar to the LasI/LasR system of *Pseudomonas aeruginosa*, but unlike *P. aeruginosa*. Whereas some strains of *P. putida* could produce only some AHLs, for example, strain WCS358 has been shown to produce only 3-oxo-C12-HSL (Bertani et al. 2004) and strain T2-2 produces both C8-HSL and C12-HSL (Chen et al. 2013). In contrast, *P. putida* KT2440 does not produce any of the common molecules involved in AHLs quorum sensing signaling described in other *Pseudomonas* (Fernández-Piñar et al. 2011) It appears that the AHLs metabolites that *P. putida* could produce are strain-specific. Consequently, whole genome sequencing of *P. putida* 6157 is required to support the results of AHLs mapping obtained from MALDI-MSI.

4.2 Experimental

Whole-genome sequencing was conducted with the illumina NovaSeq 6000 sequencing platform on genomic DNA isolated from *P. putida* 6157 to confirm the existence of the AHLs-QS system. After the raw data was obtained, *de novo* assembly was performed for genome assembly, gene prediction and gene function. Sequencing is done using a 150-bp paired-end sequencing technique generated from 1-kbp mate-pair libraries, in which the raw reads were assessed with Fasqc software, and the low-quality reads were removed using the default parameter of the Trimmomatic software. High-quality reads were subsequently assembled using SPAdes software, and the gene was called using Prokka software. The potential gene was then aligned with the reference genome sequence of *P. aeruginosa* using the Basic Local Alignment Search Tool (BLAST, NCBI) for gene annotation. Protein sequence alignments could predict if the proteins have a similar function when the pairwise sequence identity is >25% for long alignments (Rost et al. 1999).

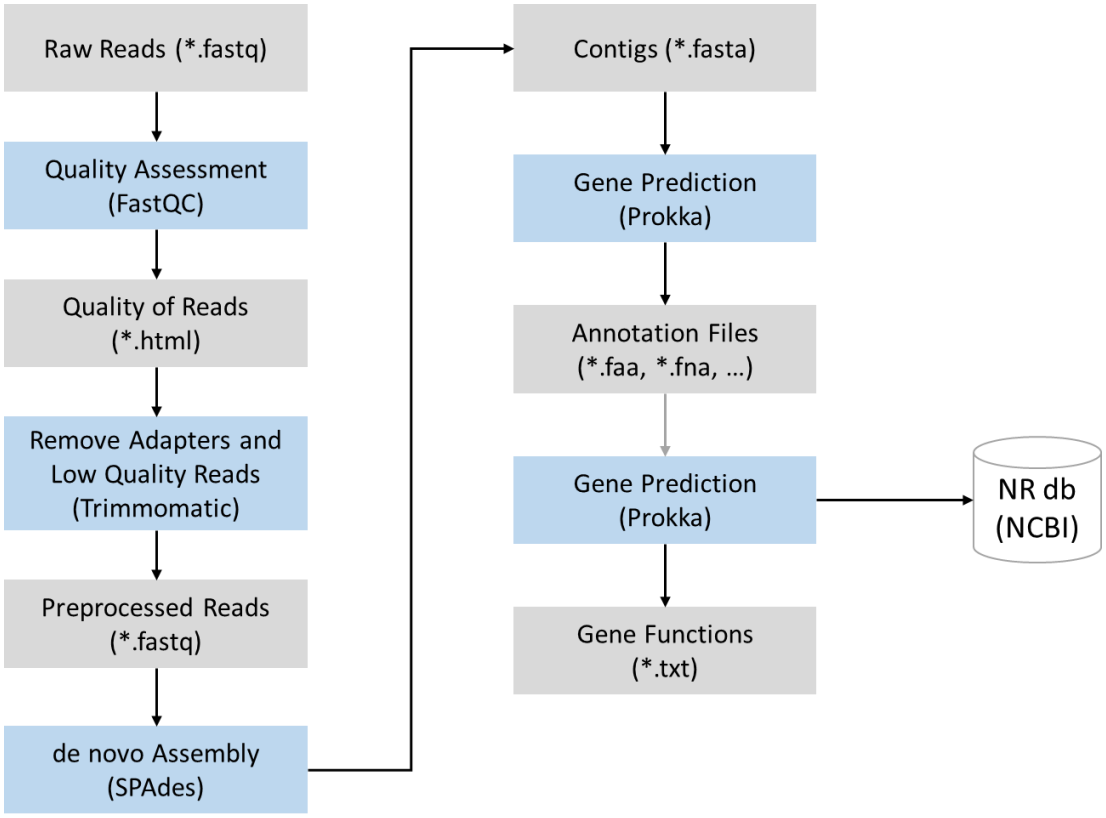

Figure 4.1 Pipeline for *de novo* assembly method

4.3 Results and Discussion

4.3.1 Genome sequencing of *P. putida* 6157

The presence of lasIR, rhlIR, and PQS clusters in the genome of *P. putida* was firstly reported by this study, leading to the production of C4-HSL, 3-oxo-C12-HSL and PQS visualized by MALDI-MSI. Genes involving AHLs-QS metabolites production with the percentage of identity of sequences producing significant alignments found in *P. putida* 6157 is presented in Table 2. Sequences producing significant alignments obtained from this work consisted of QS regulator LasR (53%), QS regulator RhlR (52%), anthranilate synthase component I (98%), anthranilate synthase component II (97%), anthranilate-CoA ligase (28%), 2-heptyl-4(1H)-quinolone synthase subunit PqsC (24%), anthraniloyl-CoA anthraniloyltransferase (29%), 2-heptyl-3-hydroxy-4(1H)-quinolone synthase (26%), QS regulator MvfR (30%), rhamnosyltransferase subunit A (93%), salicylate biosynthesis isochorismate synthase (29%), and isochorismate pyruvate lyase (31%).

Table 2 Genes involving AHLs-QS metabolites production exist in *P. putida* 6157

Genes	Sequences producing significant alignments	Identities (%)	E-value
lasR	transcriptional activator protein LasR	53	3e-21
rhlR	transcriptional activator protein LasR	52	7e-15
phnA	anthranilate synthase component I	98	0.0
phnB	anthranilate synthase component II	97	2e-145
pqsA	anthranilate-CoA ligase	28	5e-38
pqsC	2-heptyl-4(1H)-quinolone synthase subunit PqsC	24	2e-10
pqsD	anthraniloyl-CoA anthraniloyltransferase	29	3e-23
pqsH	2-heptyl-3-hydroxy-4(1H)-quinolone synthase	26	1e-19
pqsR	LysR family transcriptional regulator, quorum-sensing system regulator MvfR	30	2e-17
rhlA	rhamnosyltransferase subunit A	93	0.0
pchA	salicylate biosynthesis isochorismate synthase	29	1e-23
pchB	isochorismate pyruvate lyase	31	1e-09

4.3.2 AHLs-QS system in *P. putida* 6157

From the genome sequences, the hierarchical *N*-acyl-homoserine lactone quorum sensing system in *P. putida* 6157 biofilm was proposed as presented in Figure 4.2. LasI/LasR contains genes that produced 3-oxo-C12-HSL. While the RhlI/RhlR system generates C4-HSL. Both *las* and *rhl* have been implicated in the regulation of quinolone-like signaling molecule production in a group of *Pseudomonas* (Lee et al. 2014; Bernabè

et al. 2022). As C4-HSL and 3-oxo-C12-HSL are quinolone precursors, they could not be detected when quinolones were highly homogenously produced throughout the *P. putida*. AHL-QS are linked as LasR/3-oxo-C12-HSL is required for full expression of *pqsH*, which controls the production of PQS. The *pqs* group is repressed by the action of the RhlR/C4-HSL system. HHQ and NHQ are produced via PqsA-D system itself. Furthermore, PQS released from the cell is capable of binding iron (PQS-Fe^{3+} complex). The removal of iron by PQS induces expression of genes involved in siderophore production, leading to pyochelin production.

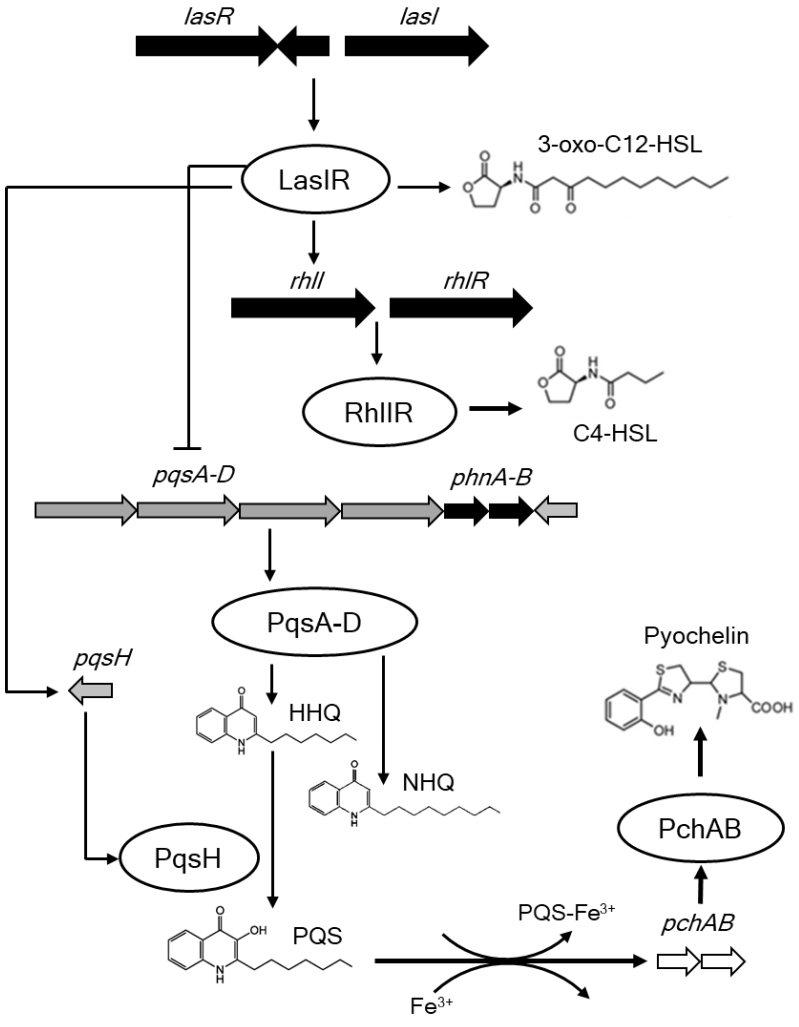

Figure 4.2 The hierarchical *N*-acyl-homoserine lactone quorum sensing system in *P. putida* 6157 biofilm

4.4 Conclusion

In this chapter, the presence of the genes responsible for the production of quorum sensing AHLs in *P. putida* 6157 was confirmed. A comprehensive genome sequencing was performed using the Illumina NovaSeq 6000 platform on genomic DNA obtained from *P. putida* 6157. The potential gene was subsequently compared to the reference genome sequence of *P. aeruginosa* through the application of the Basic Local Alignment Search Tool (BLAST, NCBI) for gene annotation. Protein sequence alignments were utilized to deduce the similarities in protein functions when the pairwise sequence identity exceeded 25% for extensive comparisons. This study marked the first time that the presence of lasIR, rhlIR, and PQS clusters in the genome of *P. putida* 6157 was reported, resulting in the detection of C4-HSL, 3-oxo-C12-HSL and PQS through MALDI-MSI visualization.

Chapter 5
Conclusion

This thesis here demonstrates the feasibility of using MALDI-MSI approach as a powerful tool to observe the spatial information of metabolites in bacterial. The agar-based biofilm workflow was developed as an optimization of biofilm cultivation and sample preparation which is convenient for MALDI-MSI analysis. The agar-based biofilm workflow for MALDI-MSI is composed of cell cultivation, adherence and formation of bacterial biofilms onto the ITO glass slide surface, pretreatment of biofilms by flash-freezing and lyophilization, matrix sublimation, and MALDI-MSI analysis and metabolite annotation to distinguish ions specific to different biofilm regions. This agar-based biofilm method is inexpensive and simple to set up, does not require the specialized equipment, and could easily be adapted to various microbial biofilms. Applying agar-based biofilm technique for MALDI-MSI, AHLs-QS metabolites were successfully visualized for the first time across *P. putida* 6157. This QS system had not been examined in previous MALDI-MSI studies of *P. putida*, perhaps due to the incompatibility of sample preparation methods. Additionally, this study revealed the relationship between biofilm development and spatial production of specific QS metabolites in *P. putida*. These findings expand our knowledge of QS and the mechanisms of AHL-QS-based biofilm formation. Furthermore, The QS metabolites identified in this study could serve as potential targets for hindering the growth of pathogenic biofilms during infection.

By applying the agar-based biofilm formation approach for MALDI-MSI developed in this study to biofilm research, we might expand our understanding of the mechanism of the biofilm development in relation to the spatial distribution of the metabolites inside. This approach is suitable for the analysis of both single species bacterial biofilms and complex microbial communities. This method might lay the groundwork for creating and testing optimal conditions for identifying biologically relevant chemical signals in microbial biofilms and other complex biological systems treated with exogenous compounds involved in infections and discovering new drugs. In addition, the developed approach can be used to study the relationship between co-

cultivation or multi-species biofilms that involve communication between bacteria, for instance, the plant co-colonization bacteria biofilms that promote plant growth and protect plants from pathogens. Utilizing the optimized method for MALDI-MSI, the foundation for interrogating the chemical topologies produced by bacteria within diverse microbiomes between bacteria species and host-bacteria might observed.

References

Baig NF, Dunham SJ, Morales-Soto N, Shrout JD, Sweedler JV, Bohn PW. Multimodal chemical imaging of molecular messengers in emerging *Pseudomonas aeruginosa* bacterial communities. Analyst. 2015 Oct 7;140(19):6544-52. doi: 10.1039/c5an01149c. Epub 2015 Sep 2. PMID: 26331158; PMCID: PMC4570871.

Bernal P, Allsopp LP, Filloux A, Llamas MA. The *Pseudomonas putida* T6SS is a plant warden against phytopathogens. ISME J. 2017 Apr;11(4):972-987. doi: 10.1038/ismej.2016.169. Epub 2017 Jan 3. PMID: 28045455; PMCID: PMC5363822.

Bernabè G, Marzaro G, Di Pietra G, Otero A, Bellato M, Pauletto A, Scarpa M, Sut S, Chilin A, Dall'Acqua S, Brun P, Castagliuolo I. A novel phenolic derivative inhibits AHL-dependent quorum sensing signaling in *Pseudomonas aeruginosa*. Front Pharmacol. 2022 Sep 20;13:996871. doi: 10.3389/fphar.2022.996871. PMID: 36204236; PMCID: PMC9531014.

Bertani I, Venturi V. Regulation of the N-acyl homoserine lactone-dependent quorum-sensing system in rhizosphere Pseudomonas putida WCS358 and cross-talk with the stationary-phase RpoS sigma factor and the global regulator GacA. Appl Environ Microbiol. 2004 Sep;70(9):5493-502. doi: 10.1128/AEM.70.9.5493-5502.2004. PMID: 15345437; PMCID: PMC520884.

Bolton N, Critchley M, Fabien R, Cromar N, Fallowfield H. Microbially influenced corrosion of galvanized steel pipes in aerobic water systems. J Appl Microbiol. 2010 Jul;109(1):239-47. doi: 10.1111/j.1365-2672.2009.04650.x. Epub 2009 Dec 10. PMID: 20070443.

Canela N, Rodríguez MÁ, Baiges I, Nadal P, Arola L. Foodomics imaging by mass spectrometry and magnetic resonance. Electrophoresis. 2016 Jul;37(13):1748-67. doi: 10.1002/elps.201500494. PMID: 26799681.

Caprioli RM, Farmer TB, Gile J. Molecular imaging of biological samples: localization of peptides and proteins using MALDI-TOF MS. Anal Chem. 1997 Dec 1;69(23):4751-60. doi: 10.1021/ac970888i. PMID: 9406525.

Cárcamo-Oyarce G, Lumjiaktase P, Kümmerli R, Eberl L. Quorum sensing triggers the stochastic escape of individual cells from Pseudomonas putida biofilms. Nat Commun. 2015 Jan 16;6:5945. doi: 10.1038/ncomms6945. PMID: 25592773; PMCID: PMC4309448.

Chen JW, Chin S, Tee KK, Yin WF, Choo YM, Chan KG. N-acyl homoserine lactone-producing Pseudomonas putida strain T2-2 from human tongue surface. Sensors (Basel). 2013 Sep 30;13(10):13192-203. doi: 10.3390/s131013192. PMID: 24084113; PMCID: PMC3859058.

Choi EN, Cho MC, Kim Y, Kim CK, Lee K. Expansion of growth substrate range in Pseudomonas putida F1 by mutations in both cymR and todS, which recruit a ring-fission hydrolase CmtE and induce the tod catabolic operon, respectively. Microbiology (Reading). 2003 Mar;149(Pt 3):795-805. doi: 10.1099/mic.0.26046-0. PMID: 12634347.

Chakraborty P, Kumar A. The extracellular matrix of mycobacterial biofilms: could we shorten the treatment of mycobacterial infections? Microb Cell. 2019 Jan 18;6(2):105-122. doi: 10.15698/mic2019.02.667. PMID: 30740456; PMCID: PMC6364259.

Crouzet M, Le Senechal C, Brözel VS, Costaglioli P, Barthe C, Bonneu M, Garbay B, Vilain S. Exploring early steps in biofilm formation: set-up of an experimental system for molecular studies. BMC Microbiol. 2014 Sep 30;14:253. doi: 10.1186/s12866-014-0253-z. PMID: 25266973; PMCID: PMC4189659.

Davies SK, Fearn S, Allsopp LP, Harrison F, Ware E, Diggle SP, Filloux A, McPhail DS, Bundy JG. Visualizing Antimicrobials in Bacterial Biofilms: Three-Dimensional Biochemical Imaging Using TOF-SIMS. mSphere. 2017 Jul 19;2(4):e00211-17. doi: 10.1128/mSphere.00211-17. PMID: 28744481; PMCID: PMC5518269.

Di Martino P. Extracellular polymeric substances, a key element in understanding biofilm phenotype. AIMS Microbiol. 2018 Mar 30;4(2):274-288. doi: 10.3934/microbiol.2018.2.274. PMID: 31294215; PMCID: PMC6604936.

Dong Y, Li B, Malitsky S, Rogachev I, Aharoni A, Kaftan F, Svatoš A, Franceschi P. Sample Preparation for Mass Spectrometry Imaging of Plant Tissues: A Review. Front Plant Sci. 2016 Feb 10;7:60. doi: 10.3389/fpls.2016.00060. PMID: 26904042; PMCID: PMC4748743.

Dunham SJ, Ellis JF, Li B, Sweedler JV. Mass Spectrometry Imaging of Complex Microbial Communities. Acc Chem Res. 2017 Jan 17;50(1):96-104. doi: 10.1021/acs.accounts.6b00503. Epub 2016 Dec 21. PMID: 28001363; PMCID: PMC5244435.

Elasri M, Delorme S, Lemanceau P, Stewart G, Laue B, Glickmann E, Oger PM, Dessaux Y. Acyl-homoserine lactone production is more common among plant-associated Pseudomonas spp. than among soilborne Pseudomonas spp. Appl Environ Microbiol. 2001 Mar;67(3):1198-209. doi: 10.1128/AEM.67.3.1198-1209.2001. PMID: 11229911; PMCID: PMC92714.

Fernández-Piñar R, Cámara M, Soriano MI, Dubern JF, Heeb S, Ramos JL, Espinosa-Urgel M. PpoR, an orphan LuxR-family protein of Pseudomonas putida KT2440, modulates competitive fitness and surface motility independently of N-acylhomoserine lactones. Environ Microbiol Rep. 2011 Feb;3(1):79-85. doi: 10.1111/j.1758-2229.2010.00190.x. PMID: 23761234.

Flemming HC, Wingender J. The biofilm matrix. Nat Rev Microbiol. 2010 Sep;8(9):623-33. doi: 10.1038/nrmicro2415. Epub 2010 Aug 2. PMID: 20676145.

Flemming HC, Wuertz S. Bacteria and archaea on Earth and their abundance in biofilms. Nat Rev Microbiol. 2019 Apr;17(4):247-260. doi: 10.1038/s41579-019-0158-9. PMID: 30760902.

Frydenlund Michelsen C, Hossein Khademi SM, Krogh Johansen H, Ingmer H, Dorrestein PC, Jelsbak L. Evolution of metabolic divergence in Pseudomonas aeruginosa during long-term infection facilitates a proto-cooperative interspecies interaction. ISME J. 2016 Jun;10(6):1323-36. doi: 10.1038/ismej.2015.220. Epub 2015 Dec 18. PMID: 26684729; PMCID: PMC5029194.

Hall-Stoodley L, Costerton JW, Stoodley P. Bacterial biofilms: from the natural environment to infectious diseases. Nat Rev Microbiol. 2004 Feb;2(2):95-108. doi: 10.1038/nrmicro821. PMID: 15040259.

Hankin JA, Barkley RM, Murphy RC. Sublimation as a method of matrix application for mass spectrometric imaging. J Am Soc Mass Spectrom. 2007 Sep;18(9):1646-52. doi: 10.1016/j.jasms.2007.06.010. Epub 2007 Jun 30. PMID: 17659880; PMCID: PMC2042488.

Heeb S, Fletcher MP, Chhabra SR, Diggle SP, Williams P, Cámara M. Quinolones: from antibiotics to autoinducers. FEMS Microbiol Rev. 2011 Mar;35(2):247-74. doi: 10.1111/j.1574-6976.2010.00247.x. PMID: 20738404; PMCID: PMC3053476.

Hendrie CA. Naloxone-sensitive hyperalgesia follows analgesia induced by morphine and environmental stimulation. Pharmacol Biochem Behav. 1989 Apr;32(4):961-6. doi: 10.1016/0091-3057(89)90066-x. PMID: 2798544.

Ikuta S, Fukusaki E, Shimma S. Visualization of Glutamate Decarboxylase Activity in Barley Seeds under Salinity Stress Using Mass Microscope. Metabolites. 2022 Dec 14;12(12):1262. doi: 10.3390/metabo12121262. PMID: 36557299; PMCID: PMC9786171.

Kaplan HB, Greenberg EP. Diffusion of autoinducer is involved in regulation of the Vibrio fischeri luminescence system. J Bacteriol. 1985 Sep;163(3):1210-4. doi: 10.1128/jb.163.3.1210-1214.1985. PMID: 3897188; PMCID: PMC219261.

Kokesch-Himmelreich J, Wittek O, Race AM, Rakete S, Schlicht C, Busch U, Römpp A. MALDI mass spectrometry imaging: From constituents in fresh food to ingredients, contaminants and additives in processed food. Food Chem. 2022 Aug 15;385:132529. doi: 10.1016/j.foodchem.2022.132529. Epub 2022 Feb 22. PMID: 35279497.

Landini P, Antoniani D, Burgess JG, Nijland R. Molecular mechanisms of compounds affecting bacterial biofilm formation and dispersal. Appl Microbiol Biotechnol. 2010 Apr;86(3):813-23. doi: 10.1007/s00253-010-2468-8. Epub 2010 Feb 18. PMID: 20165945.

Lanni EJ, Masyuko RN, Driscoll CM, Aerts JT, Shrout JD, Bohn PW, Sweedler JV. MALDI-guided SIMS: multiscale imaging of metabolites in bacterial biofilms. Anal Chem. 2014 Sep 16;86(18):9139-45. doi: 10.1021/ac5020222. Epub 2014 Aug 26. PMID: 25133532; PMCID: PMC4165220.

Lee J, Zhang L. The hierarchy quorum sensing network in Pseudomonas aeruginosa. Protein Cell. 2015 Jan;6(1):26-41. doi: 10.1007/s13238-014-0100-x. Epub 2014 Sep 25. PMID: 25249263; PMCID: PMC4286720.

Leopold J, Popkova Y, Engel KM, Schiller J. Recent Developments of Useful MALDI Matrices for the Mass Spectrometric Characterization of Lipids. Biomolecules. 2018 Dec 13;8(4):173. doi: 10.3390/biom8040173. PMID: 30551655; PMCID: PMC6316665.

Li B, Dunham SJB, Ellis JF, Lange JD, Smith JR, Yang N, King TL, Amaya KR, Arnett CM, Sweedler JV. A Versatile Strategy for Characterization and Imaging of Drip Flow Microbial Biofilms. Anal Chem. 2018 Jun 5;90(11):6725-6734. doi: 10.1021/acs.analchem.8b00560. Epub 2018 May 17. PMID: 29723465.

Lin H, Chen G, Zhao H, Cao Y. Variable metal resistance of P. putida CZ1 biofilms in different environments suggests its remediation application scope. J Environ Manage. 2021 Nov 15;298:113458. doi: 10.1016/j.jenvman.2021.113458. Epub 2021 Aug 3. PMID: 34358938.

Li X, Gu N, Huang TY, Zhong F, Peng G. Pseudomonas aeruginosa: A typical biofilm forming pathogen and an emerging but underestimated pathogen in food processing. Front Microbiol. 2023 Jan 25;13:1114199. doi: 10.3389/fmicb.2022.1114199. PMID: 36762094; PMCID: PMC9905436.

López D, Kolter R. Extracellular signals that define distinct and coexisting cell fates in Bacillus subtilis. FEMS Microbiol Rev. 2010 Mar;34(2):134-49. doi: 10.1111/j.1574-6976.2009.00199.x. Epub 2009 Nov 23. PMID: 20030732.

Molina-Santiago C, Pearson JR, Navarro Y, Berlanga-Clavero MV, Caraballo-Rodriguez AM, Petras D, García-Martín ML, Lamon G, Haberstein B, Cazorla FM, de Vicente A, Loquet A, Dorrestein PC, Romero D. The extracellular matrix protects Bacillus subtilis colonies from Pseudomonas invasion and modulates plant co-colonization. Nat Commun. 2019 Apr 23;10(1):1919. doi: 10.1038/s41467-019-09944-x. PMID: 31015472; PMCID: PMC6478825.

Moore JL, Caprioli RM, Skaar EP. Advanced mass spectrometry technologies for the study of microbial pathogenesis. Curr Opin Microbiol. 2014 Jun;19:45-51. doi: 10.1016/j.mib.2014.05.023. Epub 2014 Jul 3. PMID: 24997399; PMCID: PMC4125470.

Nathwani D, Raman G, Sulham K, Gavaghan M, Menon V. Clinical and economic consequences of hospital-acquired resistant and multidrug-resistant Pseudomonas aeruginosa infections: a systematic review and meta-analysis. Antimicrob Resist Infect Control. 2014 Oct 20;3(1):32. doi: 10.1186/2047-2994-3-32. PMID: 25371812; PMCID: PMC4219028.

Ng WL, Bassler BL. Bacterial quorum-sensing network architectures. Annu Rev Genet. 2009;43:197-222. doi: 10.1146/annurev-genet-102108-134304. PMID: 19686078; PMCID: PMC4313539.

Norris JL, Caprioli RM. Analysis of tissue specimens by matrix-assisted laser desorption/ionization imaging mass spectrometry in biological and clinical research. Chem Rev. 2013 Apr 10;113(4):2309-42. doi: 10.1021/cr3004295. Epub 2013 Feb 11. PMID: 23394164; PMCID: PMC3624074.

Novick RP, Ross HF, Projan SJ, Kornblum J, Kreiswirth B, Moghazeh S. Synthesis of staphylococcal virulence factors is controlled by a regulatory RNA molecule. EMBO J. 1993 Oct;12(10):3967-75. doi: 10.1002/j.1460-2075.1993.tb06074.x. PMID: 7691599; PMCID: PMC413679.

Novick RP, Projan SJ, Kornblum J, Ross HF, Ji G, Kreiswirth B, Vandenesch F, Moghazeh S. The agr P2 operon: an autocatalytic sensory transduction system in Staphylococcus aureus. Mol Gen Genet. 1995 Aug 30;248(4):446-58. doi: 10.1007/BF02191645. PMID: 7565609.Pearson JP, Van Delden C, Iglewski BH. Active efflux and diffusion are involved in transport of Pseudomonas aeruginosa cell-to-cell signals. J Bacteriol. 1999 Feb;181(4):1203-10. doi: 10.1128/JB.181.4.1203-1210.1999. PMID: 9973347; PMCID: PMC93498.

Ma LZ, Wang D, Liu Y, Zhang Z, Wozniak DJ. Regulation of Biofilm Exopolysaccharide Biosynthesis and Degradation in Pseudomonas aeruginosa. Annu Rev Microbiol. 2022 Sep 8;76:413-433. doi: 10.1146/annurev-micro-041320-111355. Epub 2022 Jun 2. PMID: 35655342.

Pang Z, Raudonis R, Glick BR, Lin TJ, Cheng Z. Antibiotic resistance in Pseudomonas aeruginosa: mechanisms and alternative therapeutic strategies. Biotechnol Adv. 2019 Jan-Feb;37(1):177-192. doi: 10.1016/j.biotechadv.2018.11.013. Epub 2018 Nov 27. PMID: 30500353.

Phelan VV, Fang J, Dorrestein PC. Mass Spectrometry Analysis of Pseudomonas aeruginosa Treated with Azithromycin. J Am Soc Mass Spectrom. 2015 Jun;26(6):873-7. doi: 10.1007/s13361-015-1101-6. Epub 2015 Mar 24. PMID: 25801585; PMCID: PMC4425625.

Powers MJ, Sanabria-Valentín E, Bowers AA, Shank EA. Inhibition of Cell The extracellular matrix protects Bacillus subtilis colonies from Pseudomonas invasion and modulates plant co-colonization. J Bacteriol. 2013 Jul;197(13):2129-2138. doi: 10.1128/JB.02535-14. Epub 2013 Mar 30. PMID: 25825426; PMCID: PMC4455266.

Purtschert-Montenegro G, Cárcamo-Oyarce G, Pinto-Carbó M, Agnoli K, Bailly A, Eberl L. Pseudomonas putida mediates bacterial killing, biofilm invasion and biocontrol with a type IVB secretion system. Nat Microbiol. 2022 Oct;7(10):1547-1557. doi: 10.1038/s41564-022-01209-6. Epub 2022 Sep 19. PMID: 36123439; PMCID: PMC9519443.

Rodrigues AMS, Lami R, Escoubeyrou K, Intertaglia L, Mazurek C, Doberva M, Pérez-Ferrer P, Stien D. Straightforward N-Acyl Homoserine Lactone Discovery and Annotation by LC-MS/MS-based Molecular Networking. J Proteome Res. 2022 Mar 4;21(3):635-642. doi: 10.1021/acs.jproteome.1c00849. Epub 2022 Feb 1. PMID: 35102742.

Rost B. Twilight zone of protein sequence alignments. Protein Eng. 1999 Feb;12(2):85-94. doi: 10.1093/protein/12.2.85. PMID: 10195279.

Ruhal R, Kataria R. Biofilm patterns in gram-positive and gram-negative bacteria. Microbiol Res. 2021 Oct;251:126829. doi: 10.1016/j.micres.2021.126829. Epub 2021 Jul 23. PMID: 34332222.

Sauer K, Stoodley P, Goeres DM, Hall-Stoodley L, Burmølle M, Stewart PS, Bjarnsholt T. The biofilm life cycle: expanding the conceptual model of biofilm formation. Nat Rev Microbiol. 2022 Oct;20(10):608-620. doi: 10.1038/s41579-022-00767-0. Epub 2022 Aug 3. PMID: 35922483; PMCID: PMC9841534.

Skariyachan S, Sridhar VS, Packirisamy S, Kumargowda ST, Challapilli SB. Recent perspectives on the molecular basis of biofilm formation by Pseudomonas aeruginosa and approaches for treatment and biofilm dispersal. Folia Microbiol (Praha). 2018 Jul;63(4):413-432. doi: 10.1007/s12223-018-0585-4. Epub 2018 Jan 19. PMID: 29352409.

Seed PC, Passador L, Iglewski BH. Activation of the Pseudomonas aeruginosa lasI gene by LasR and the Pseudomonas autoinducer PAI: an autoinduction regulatory hierarchy. J Bacteriol. 1995 Feb;177(3):654-9. doi: 10.1128/jb.177.3.654-659.1995. PMID: 7836299; PMCID: PMC176640.

Shimma S. Mass Spectrometry Imaging. Mass Spectrom (Tokyo). 2022;11(1):A0102. doi: 10.5702/massspectrometry.A0102. Epub 2022 Feb 25. PMID: 35291501; PMCID: PMC8900255.

Si T, Li B, Zhang K, Xu Y, Zhao H, Sweedler JV. Characterization of Bacillus subtilis Colony Biofilms via Mass Spectrometry and Fluorescence Imaging. J Proteome Res. 2016 Jun 3;15(6):1955-62. doi: 10.1021/acs.jproteome.6b00127. Epub 2016 May 11. PMID: 27136705; PMCID: PMC4895246.

Steidle A, Sigl K, Schuhegger R, Ihring A, Schmid M, Gantner S, Stoffels M, Riedel K, Givskov M, Hartmann A, Langebartels C, Eberl L. Visualization of N-acylhomoserine lactone-mediated cell-cell communication between bacteria colonizing the tomato rhizosphere. Appl Environ Microbiol. 2001 Dec;67(12):5761-70. doi: 10.1128/AEM.67.12.5761-5770.2001. PMID: 11722933; PMCID: PMC93370.

Steidle A, Allesen-Holm M, Riedel K, Berg G, Givskov M, Molin S, Eberl L. Identification and characterization of an N-acylhomoserine lactone-dependent quorum-sensing system in Pseudomonas putida strain IsoF. Appl Environ Microbiol. 2002 Dec;68(12):6371-82. doi: 10.1128/AEM.68.12.6371-6382.2002. PMID: 12450862; PMCID: PMC134430.

Sugiura Y, Shimma S, Setou, M. Thin sectioning improves the peak intensity and signal-to-noise ratio in direct tissue mass spectrometry. J. Mass Spectrom. Soc. Jpn. 2006 54, 45–48. Available at: https://doi.org/10.5702/massspec.54.45.(2006).

Suma MS, Basheer R, Sreelekshmy BR, Vipinlal V, Sha MA, Jineesh P, Shibli SMA. Pseudomonas putida RSS biopassivation of mild steel for long term corrosion inhibition. Int. Biodeterior. Biodegradation. 2019 137, 59-67.

Takeo E, Sugiura Y, Ohnishi Y, Kishima H, Fukusaki E, Shimma S. Mass Spectrometric Enzyme Histochemistry for Choline Acetyltransferase Reveals De Novo Acetylcholine Synthesis in Rodent Brain and Spinal Cord. ACS Chem Neurosci. 2021 Jun 16;12(12):2079-2087. doi: 10.1021/acschemneuro.0c00720. Epub 2021 Jun 2. PMID: 34078081.

Tolker-Nielsen T. Biofilm Development. Microbiol Spectr. 2015 Apr;3(2):MB-0001-2014. doi: 10.1128/microbiolspec.MB-0001-2014. PMID: 26104692.

Tuon FF, Dantas LR, Suss PH, Tasca Ribeiro VS. Pathogenesis of the Pseudomonas aeruginosa Biofilm: A Review. Pathogens. 2022 Feb 27;11(3):300. doi: 10.3390/pathogens11030300. PMID: 35335624; PMCID: PMC8950561.

Turkina MV, Vikström E. Bacteria-Host Crosstalk: Sensing of the Quorum in the Context of Pseudomonas aeruginosa Infections. J Innate Immun. 2019;11(3):263-279. doi: 10.1159/000494069. Epub 2018 Nov 14. PMID: 30428481; PMCID: PMC6738176.

van Gestel J, Vlamakis H, Kolter R. Division of Labor in Biofilms: the Ecology of Cell Differentiation. Microbiol Spectr. 2015 Apr;3(2):MB-0002-2014. doi: 10.1128/microbiolspec.MB-0002-2014. PMID: 26104716.

Venturi V. Regulation of quorum sensing in Pseudomonas. FEMS Microbiol Rev. 2006 Mar;30(2):274-91. doi: 10.1111/j.1574-6976.2005.00012.x. PMID: 16472307.

Verstraeten N, Braeken K, Debkumari B, Fauvart M, Fransaer J, Vermant J, Michiels J. Living on a surface: swarming and biofilm formation. Trends Microbiol. 2008 Oct;16(10):496-506. doi: 10.1016/j.tim.2008.07.004. Epub 2008 Sep 3. PMID: 18775660.

Vickerman JC. Molecular imaging and depth profiling by mass spectrometry--SIMS, MALDI or DESI? Analyst. 2011 Jun 7;136(11):2199-217. doi: 10.1039/c1an00008j. Epub 2011 Apr 4. PMID: 21461433.

Wakeman CA, Moore JL, Noto MJ, Zhang Y, Singleton MD, Prentice BM, Gilston BA, Doster RS, Gaddy JA, Chazin WJ, Caprioli RM, Skaar EP. The innate immune protein calprotectin promotes Pseudomonas aeruginosa and Staphylococcus aureus interaction. Nat Commun. 2016 Jun 15;7:11951. doi: 10.1038/ncomms11951. PMID: 27301800; PMCID: PMC4912628.

Wei Y, Perez LJ, Ng WL, Semmelhack MF, Bassler BL. Mechanism of Vibrio cholerae autoinducer-1 biosynthesis. ACS Chem Biol. 2011 Apr 15;6(4):356-65. doi: 10.1021/cb1003652. Epub 2011 Jan 13. PMID: 21197957; PMCID: PMC3077805.

Weimer A, Kohlstedt M, Volke DC, Nikel PI, Wittmann C. Industrial biotechnology of Pseudomonas putida: advances and prospects. Appl Microbiol Biotechnol. 2020 Sep;104(18):7745-7766. doi: 10.1007/s00253-020-10811-9. Epub 2020 Aug 13. PMID: 32789744; PMCID: PMC7447670.

Yang JY, Phelan VV, Simkovsky R, Watrous JD, Trial RM, Fleming TC, Wenter R, Moore BS, Golden SS, Pogliano K, Dorrestein PC. Primer on agar-based microbial imaging mass spectrometry. J Bacteriol. 2012 Nov;194(22):6023-8. doi: 10.1128/JB.00823-12. Epub 2012 Jul 20. PMID: 22821974; PMCID: PMC3486372.

Yang YL, Xu Y, Straight P, Dorrestein PC. Translating metabolic exchange with imaging mass spectrometry. Nat Chem Biol. 2009 Dec;5(12):885-7. doi: 10.1038/nchembio.252. Epub 2009 Nov 8. PMID: 19915536; PMCID: PMC2778862.

List of Publications

Original papers

Pitchapa R, Dissook S, Putri SP, Fukusaki E, Shimma S. MALDI Mass Spectrometry Imaging Reveals the Existence of an *N*-Acyl-homoserine Lactone Quorum Sensing System in Pseudomonas putida Biofilms. Metabolites. 2022 Nov 21;12(11):1148. doi: 10.3390/metabo12111148. PMID: 36422288; PMCID: PMC9697013.

Conference list

Rattanaburi Pitchapa, Eiichiro Fukusaki, Shuichi Shimma. Mass spectrometry imaging reveals the correlation between the production of quorum sensing metabolites and the biofilm development in *Pseudomonas putida* biofilms. Japan Society for Bioscience, Biotechnology, and Agrochemistry Annual Meeting (2019) – Poster and oral presentation.

Appendices

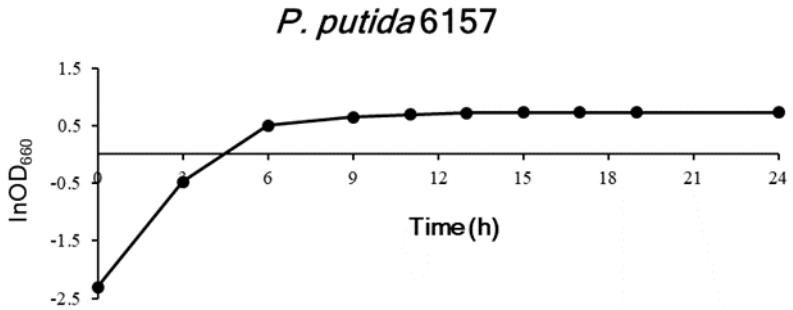

Figure S1. Growth profile of *P. putida* 6157

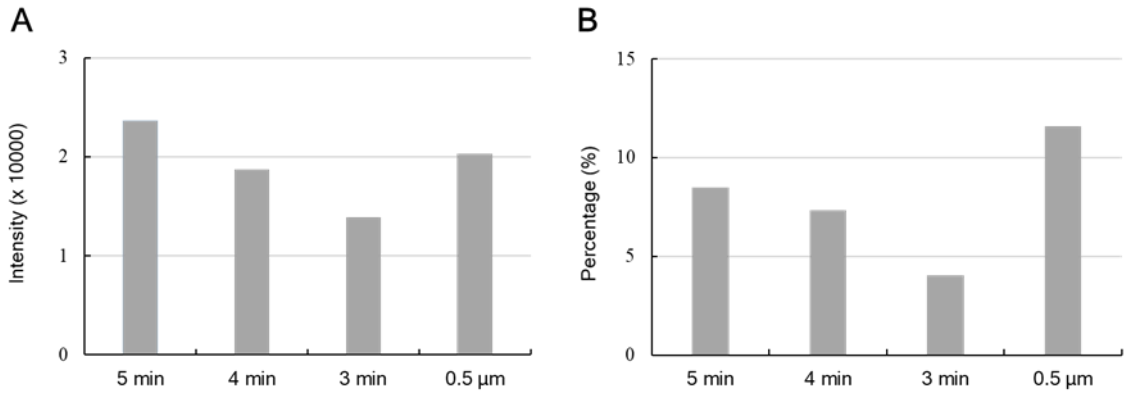

Figure S2. The effect of matrix thickness and sublimated time towards peak intensity of *m/z* 325.07 (A) and the percentage compared to highest matrix peak; *m/z* 273.04 (B)

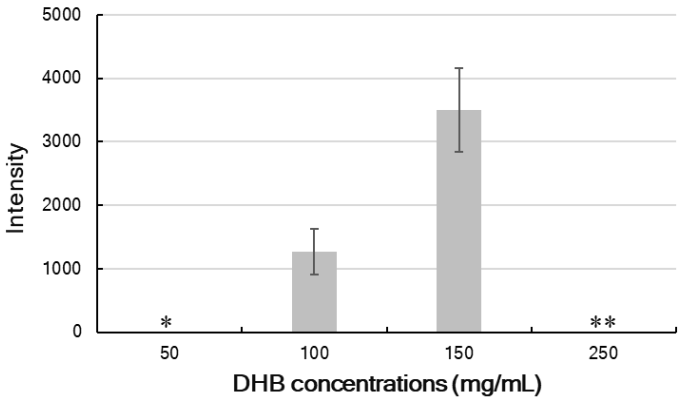

Figure S3. Effect of DHB concentrations on the peak intensity (n=3) of *m/z* 325.07. No *m/z* 325.07 was detected (*). The air brush was clogged due to a high concentration of DHB (**)

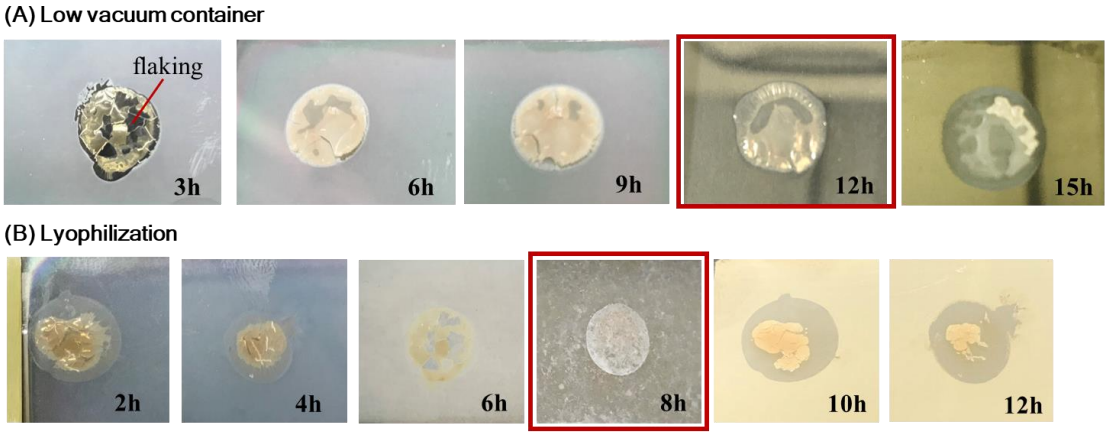

Figure S4. The biofilm morphology during biofilm processing *via* (A) low vacuum container and (B) lyophilization. The optimized time for dehydration were selected at 12 and 8 hours, respectively (red boxes).

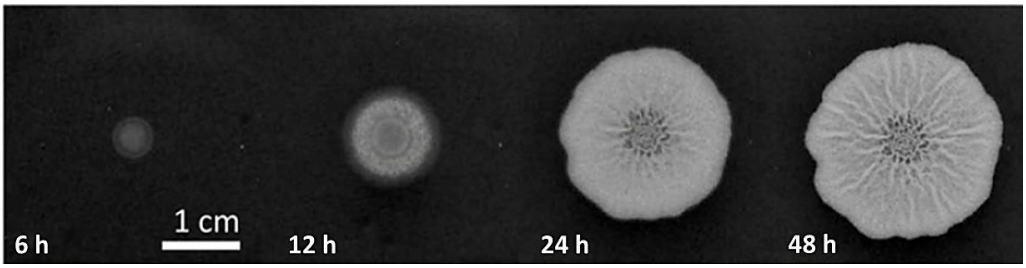

Figure S5. *P. putida* 6157 biofilms cultivated by agar-based biofilm method at 6, 12, 24, and 48 hours after inoculation. The biofilm increases in height to hundreds of micrometers, spreads to reach a diameter of several centimeters, and forms macroscopic wrinkles as swarming motality.

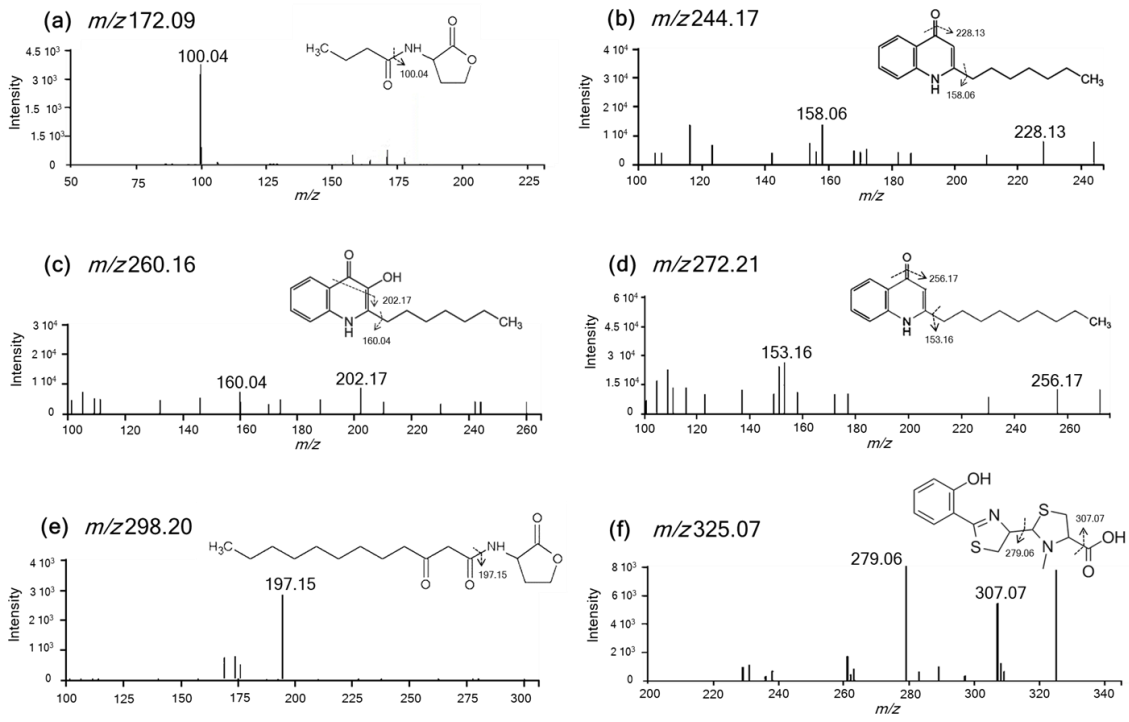

Figure S6. Annotation of QS metabolites via tandem mass spectra of *m/z* values highlighted in Figure 3.1

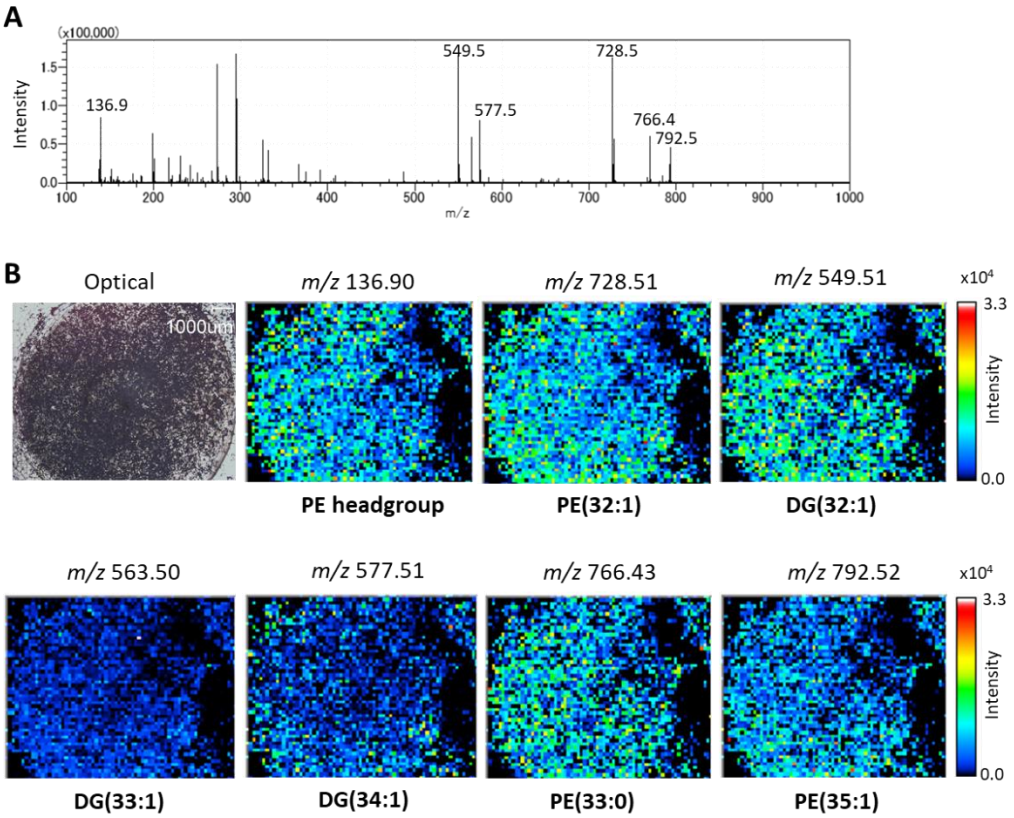

Figure S7. Representative MALDI-ToF spectra and ion images of a *P. putida* at 48 h after biofilm formation

Genome sequences of genes involving AHLs-QS system

lasR

EIEPPJPH_02187 Transcriptional activator protein LasR

Length=82

Score = 82.0 bits (201), Expect = 3e-21, Method: Compositional matrix adjust.

Identities = 37/70 (53%), Positives = 47/70 (67%), Gaps = 0/70 (0%)

```
Query  168  EHPVSKPVVLTSREKEVLQWCAIGKTSWEISVICNCSEANVNFHMGNIRRKFGVTSRRVA  227
            + PV  PV LT RE++VL WCA GK+SWEI  I  C E+ VNFH+ NI RKF V +R  A
Sbjct  10    QPPVDAPVRLTPRERQVLLWCAYGKSSWEIGRILECKESTVNFHVSNILRKFDVPTRVAA  69
Query  228  AIMAVNLGLI  237
            I A+  G++
Sbjct  70    VIKAIRYGML  79
```

rhlR

EIEPPJPH_02187 Transcriptional activator protein LasR

Length=82

Score = 65.5 bits (158), Expect = 7e-15, Method: Compositional matrix adjust.

Identities = 33/64 (52%), Positives = 40/64 (63%), Gaps = 0/64 (0%)

```
Query  178  PVCLSHREREILQWTADGKSSGEIAIILSISESTVNFHHKNIQKKFDAPNKTLAAAYAAA  237
            PV L+ RER++L W A GKSS EI  IL   ESTVNFH  NI +KFD P +  A   A
Sbjct  16    PVRLTPRERQVLLWCAYGKSSWEIGRILECKESTVNFHVSNILRKFDVPTRVAAVIKAIR  75
Query  238  LGLI  241
              G++
Sbjct  76    YGML  79
```

phnA

EIEPPJPH_05146 Anthranilate synthase component 1

Length=493

Score = 991 bits (2563), Expect = 0.0, Method: Compositional matrix adjust.

Identities = 485/493 (98%), Positives = 489/493 (99%), Gaps = 0/493 (0%)

```
Query  1    MNREEFLRLAAAGYNRIPLACETLADFDTPLSIYLKLADQPNSYLLESVQGGEKWGRYSM  60
            MNREEFLRLAA GYNRIPLACETLADFDTPLSIYLKLADQPNSYLLESVQGGEKWGRYSM
Sbjct  1    MNREEFLRLAAVGYNRIPLACETLADFDTPLSIYLKLADQPNSYLLESVQGGEKWGRYSM  60
Query  61   IGLPSRTVMRVHGYRVSILHDGVEVESCEVEDPLAFVETFKDRYKVADIPGLPRFNGGLV  120
            IGLPSRTVMRVHGY VSILHDGVEVES +VEDPLAFVE+FKDRYKVADIPGLPRFNGGLV
Sbjct  61   IGLPSRTVMRVHGYHVSILHDGVEVESHDVEDPLAFVESFKDRYKVADIPGLPRFNGGLV  120
Query  121  GYFGYDCVRYVEKRLGASPNPDPLGVPDILLMVSDAVVVFDNLAGKMHAIVLVDPAEDQA  180
            GYFGYDCVRYVEKRLGASPNPDPLGVPDILLMVSDAVVVFDNLAGKMHAIVLVDPAE+QA
Sbjct  121  GYFGYDCVRYVEKRLGASPNPDPLGVPDILLMVSDAVVVFDNLAGKMHAIVLVDPAEEQA  180
```

Query 181 FEQGQARLQGLLETLRQPITPRRGLDLSGPQAAEPAFRSSYTREDYENAVGRIKEYILAG 240
FEQGQARLQGLLETLRQPITPRRGLDLSGPQAAEP FRSSYTREDYENAVGRIKEYILAG
Sbjct 181 FEQGQARLQGLLETLRQPITPRRGLDLSGPQAAEPEFRSSYTREDYENAVGRIKEYILAG 240
Query 241 DCMQVVPSQRMSIDFKAAPIDLYRALRCFNPTPYMYFFNFGDFHVVGSSPEVLVRVEDNL 300
DCMQVVPSQRMSIDFKAAPIDLYRALRCFNPTPYMYFFNFGDFHVVGSSPEVLVRVEDNL
Sbjct 241 DCMQVVPSQRMSIDFKAAPIDLYRALRCFNPTPYMYFFNFGDFHVVGSSPEVLVRVEDNL 300
Query 301 VTVRPIAGTRPRGATEEADRALEDDLLSDDKEIAEHLMLIDLGRNDVGRVSSTGSVRLTE 360
VTVRPIAGTRPRGATEEADRALEDDLLSDDKEIAEHLMLIDLGRNDVGRVSSTGSVRLTE
Sbjct 301 VTVRPIAGTRPRGATEEADRALEDDLLSDDKEIAEHLMLIDLGRNDVGRVSSTGSVRLTE 360
Query 361 KMVIERYSNVMHIVSNVTGQLREGLTAMDALRAILPAGTLSGAPKIRAMEIIDELEPVKR 420
KMVIERYSNVMHIVSNVTGQLREGLTAMDALRAILPAGTLSGAPKIRAMEIIDELEPVKR
Sbjct 361 KMVIERYSNVMHIVSNVTGQLREGLTAMDALRAILPAGTLSGAPKIRAMEIIDELEPVKR 420
Query 421 GVYGGAVGYFAWNGNMDTAIAIRTAVIKDGELHVQAGGGIVADSVPALEWEETINKRRAM 480
GVYGGAVGYFAWNGNMDTAIAIRTAVIKDGELHVQAGGGIVADSVPALEWEETINKRRAM
Sbjct 421 GVYGGAVGYFAWNGNMDTAIAIRTAVIKDGELHVQAGGGIVADSVPALEWEETINKRRAM 480
Query 481 FRAVALAEQTSAR 493
FRAVALAEQTSA+
Sbjct 481 FRAVALAEQTSAK 493

phnB

EIEPPJPH_05144 Anthranilate synthase component 2

Length=197

Score = 399 bits (1026), Expect = 2e-145, Method: Compositional matrix adjust.

Identities = 192/197 (97%), Positives = 194/197 (98%), Gaps = 0/197 (0%)

Query 1 MLLMIDNYDSFTYNVVQYLGELGAEVKVIRNDEMTIAQIEALNPERIVVSPGPCTPSEAG 60
MLLMIDNYDSFTYNVVQYLGELGAEVKVIRNDEMTIAQIEALNPERIVVSPGPCTPSEAG
Sbjct 1 MLLMIDNYDSFTYNVVQYLGELGAEVKVIRNDEMTIAQIEALNPERIVVSPGPCTPSEAG 60
Query 61 VSIEAILHFAGKLPILGVCLGHQSIGQAFGGDVVRARQVMHGKTSPVYHRDLGVFASLNN 120
VSIEAILHFAGKLPILGVCLGHQSIGQAFGGDVVRARQVMHGKTSPV+HRDLGVF LNN
Sbjct 61 VSIEAILHFAGKLPILGVCLGHQSIGQAFGGDVVRARQVMHGKTSPVHHRDLGVFTGLNN 120
Query 121 PLTVTRYHSLVVKRETLPDCLEVTAWTSHADGSVDEIMGLRHKTLNIEGVQFHPESILTE 180
PLTVTRYHSLVVKRETLPDCLEVTAWT+H DGSVDEIMGLRHKTLNIEGVQFHPESILTE
Sbjct 121 PLTVTRYHSLVVKRETLPDCLEVTAWTAHEDGSVDEIMGLRHKTLNIEGVQFHPESILTE 180
Query 181 QGHELFANFLKQTGGRR 197
QGHELFANFLKQTGGRR
Sbjct 181 QGHELFANFLKQTGGRR 197

pqsA

EIEPPJPH_03565 anthranilate-CoA ligase

Length=560

Score = 144 bits (364), Expect = 5e-38, Method: Compositional matrix adjust.

Identities = 152/535 (28%), Positives = 241/535 (45%), Gaps = 46/535 (9%)

```
Query  40   LAASAARHPRRIALCDDDQ-RLSYADLLQRCRRLAAGLRQAGLAHGDTVVLHLPNGIAFV  98
            L  S +R+ +   +   DQ RL+Y  L +R  RLA  L +AG+  GDTV +   +  ++
Sbjct  23   LLMSGSRYEKTREIVYRDQLRLTYPQLNERIARLANVLTEAGVKAGDTVAVMDWDSHRYL  82
Query  99   ETCFALFQLGVRPVLALPAHRQHEISGFCRFAEAKA------YIGA-ERIDGFDPRPMAR  151
            E  FA+  +G           +I     AE +      ++G  + I G
Sbjct  83   ECMFAIPMIGAVVHTINVRLSPEQILYTMNHAEDRVVLVNSDFVGLYQGIAGQLTTVDKT  142

Query  152  ELLASGACRMALIH---GEAEAPLQALAPLYQADALEDCAARAEDIACFQLSGGTTGTPK  208
              LL  G  + A +    GE E  L A +P Y    ++ +    +A    + GTTG PK
Sbjct  143  LLLTDGPDKTAELPDLVGEYEQLLAAASPHYDFPDFDENS-----VATTFYTTGTTGNPK  197
Query  209  LIPRRHREYLYNVRASAEVCG-------FDEHTVYLTGLPMAHNFTLCCPGVIGTLLAGG  261
            +   HR+ + +  A A V G         + VY+   PM H     P     + G
Sbjct  198  GVYFTHRQLVLHTLAEASVTGSIDSVRLLGSNDVYMPITPMFHVHAWGIP--YAATMLGM  255
Query  262  RVVVSQRADPEHCFALIARERVTHTALVPPLAMLWLDAQESRRADLSSLRLLQVGGSRLG  321
            + V   R +P+    L   E+VT +  VP +  + L+   S+  D    +++ +GGS L
Sbjct  256  KQVYPGRYEPDMLVKLWREEKVTFSHCVPTILQMLLNCPTSQGQDFGGWKII-IGGSALN  314
Query  322  SSAAQRVEPVLGCQLQQVLGMAEG--LICYTRLDDP------PERVLH--TQGRPLSPDD  371
            S  Q     G QL    GM+E   LI    L+D       ER+ +    G P+ P
Sbjct  315  RSLYQ-AALARGIQLTAAYGMSETCPLISAAHLNDELQAGSEDERITYRIKAGVPV-PLV  372
Query  372  EVRVVDAEGREV-GPGEV-GELTVRGPYTIRGYYRLPEHNAKAFSADGFYRTGDRVSRDK  429
             E  +VD +G  +   GE  GEL +R P+   GY++ PE + + +   G+  TGD  + D
Sbjct  373  EAAIVDGDGNFLPSDGETQGELVLRAPWLTMGYFKEPEKSEELWQG-GWLHTGDVATLDG  431
Query  430  DGYLVVEGRDKDQINRGGEKIAAEEVENLLIAHPQVHDATVVAMPDSLLGERTCAFVIPR  489
             GY+ +  R KD I  GGE I++ ++E+L+  HP V +  VV + D   GER  A ++ R
Sbjct  432  MGYIDIRDRIKDVIKTGGEWISSLDLEDLISRHPAVREVAVVGVADPQWGERPFALLVVR  491
Query  490  QPA---PSALK--LKQYLHACGLAAFKVPDRIELVPAFPQTGIGKISKKDLRERL  539
             ALK  LK ++    +  + +P +I +V   P+T +GK+ GK KK +R+ +
Sbjct  492  DGQAIDAKALKEHLKPFVEQGHINKWAIPSQIAVVTEVPKTSVGKLDKKRIRQDI  546
```

pqsC

EIEPPJPH_03779 3-oxoacyl-[acyl-carrier-protein] synthase 3

Length=311

Score = 58.5 bits (140), Expect = 2e-10, Method: Compositional matrix adjust.

Identities = 71/299 (24%), Positives = 128/299 (43%), Gaps = 42/299 (14%)

```
Query  47   FDPRNGENEFS--LVVRAAERLLRSSDTA-PDSVDMLICSASSPIMTDAGDVLPDLRGRL  103
            F PR   N+ +  L V AA+ L  ++ +  P ++D +I     ++T  GD
Sbjct  40   FLPRKDANQETSDLCVEAAQALFAANPSLDPAAIDAVI------VVTQNGDA------EG  87
Query  104  YPRMANVLSKQLGLSRALP-LDSQMECASFLLNLRLAASMIRQGKAEKVLVVCSEYISNL  162
              P  A ++  +LGLS A+   D  + C+ ++  L     +   + L++ ++  S +
Sbjct  88   LPHTAAIVQHKLGLSTAVAAFDISLGCSGYVYGLYAMKGFMEAAGLKNGLLITADPYSKI  147
Query  163  LDFTSRTST-LFADGCAVALLTRGDDDSCDLLASAEHSDATFYEVATGRWRLPENPTGEA  221
            +D   R +T LF D     +  G+D +  L  S   SD    E     R  +
Sbjct  148  VDPEDRNTTMLFGDAATATWM--GEDAAWQLGKSLFGSDGAGAE----HLRTTDGK----  197
Query  222  KPRLYFSLFSDGQNKMASFVPTNVPIAMRRALEKAGLGSDDIDYFVFHQPAPFLVKAWAE  281
            F +G+ ++ +F    VP  +++ LE + L ++DID +  HQ +  +V A +
Sbjct  198  -------FFMNGR-QVYNFALVKVPAHLQQLLEASALQAEDIDLYCLHQGSAAIVDAVSS  249
Query  282  GI--GARPEQYQLTMGDTGVMISVSIPYTLMTGLREGKIRPGDRIVMAGAATG--WGFA  336
            G   +++   M +TG  +S SIP  L   +   + R+ ++G  G  WG A
Sbjct  250  RFDEGEHKQKFVKDMVETGNTVSSSIPLLLEKHVLGSSCK---RVALSGFGVGLSWGSA  305
```

pqsD

EIEPPJPH_03779 3-oxoacyl-[acyl-carrier-protein] synthase 3

Length=311

Score = 95.5 bits (236), Expect = 3e-23, Method: Compositional matrix adjust.

Identities = 96/326 (29%), Positives = 143/326 (44%), Gaps = 36/326 (11%)

```
Query  13   LPKRQVSNHDLVGRINTSDEFIVERTGVRTRYHVEPEQAVSALMVPAARQAIEAAG--LL  70
            +P   V N+   +    EFI  + G      + Q  S L V AA QA+ AA   L
Sbjct  11   VPVNGVDNYAQGAKFGKDQEFIFGKIGSTFLPRKDANQETSDLCVEAA-QALFAANPSLD  69
Query  71   PEDIDLLLVNTLSPDHHD-PSQACLIQPLLGLRH-IPVLDIRAQCSGLLYGLQMARGQIL  128
            P  ID ++V T + D    P  A ++Q  LGL   +   DI   CSG +YGL   +G +
Sbjct  70   PAAIDAVIVVTQNGDAEGLPHTAAIVQHKLGLSTAVAAFDISLGCSGYVYGLYAMKGFME  129
Query  129  AGLARHVLVVCGEVLSKRMDCSDRGRNLSILLGDGAGAVVVSAGESLEDGLLDLRLGADG  188
              A  ++ L++  +  SK +D  DR  N ++L GD A A  +  GE     L     G+DG
Sbjct  130  AAGLKNGLLITADPYSKIVDPEDR--NTTMLFGDAATATWM--GEDAAWQLGKSLFGSDG  185
Query  189  NYFDLLMTAAPGSASPTFLDENVLREGGGEFLMRGRPMFEHASQTLVRIAG---EMLAAH  245
                    LR   G+F M GR ++  A   LV++    ++L A
Sbjct  186  ------------------AGAEHLRTTDGKFFMNGRQVYNFA---LVKVPAHLQQLLEAS  224
Query  246  ELTLDDIDHVICHQPNLRILDAVQEQLGIPQH--KFAVTVDRLGNMASASTPVTLAMFWP  303
              L  +DID    HQ +  I+DAV  +   +H  KF   +  GN  S+S P+ L
Sbjct  225  ALQAEDIDLYCLHQGSAAIVDAVSSRFDEGEHKQKFVKDMVETGNTVSSSIPLLLEKHVL  284
```

Query 304 DIQPGQRVLVLTYGSGATWGAALYRK 329
+RV + +G G +WG+A+ +
Sbjct 285 G-SSCKRVALSGFGVGLSWGSAIIER 309

pqsH

EIEPPJPH_02023 6-hydroxynicotinate 3-monooxygenase

Length=382

Score = 87.0 bits (214), Expect = 1e-19, Method: Compositional matrix adjust.

Identities = 81/310 (26%), Positives = 131/310 (42%), Gaps = 37/310 (12%)

Query 23 GIDWLLVERASEIRPIGTGITLASNALT-----ALSSTLDL-----DRLFRRGMPLAGIN 72
G D + E+A E +G GI + N + L L+L D F R
Sbjct 27 GFDVEVFEQAPEFTRLGAGIHIGPNVMKIFRRMGLEQKLELMGSHPDFWFSRD------- 79
Query 73 VYAHDGSMLMSMPSSLGGNSR-----GGLALQRHELHAALLEGLDESRIRVGVSIVQILD 127
+ G L +P LG +R + + R +LHA ++ + + G + +I+D
Sbjct 80 --GNTGDYLSRIP--LGEYARREYGAAYITIHRGDLHALQIDAIKPGTVHFGKRLQKIVD 135
Query 128 GLDHERVTLSDGTVHDCSLVVGADGIRSSVRRYVWPEATLRHSGETCWRLVV-----PHR 182
D R+ +DGT +V+GADGI S +R + +SG R ++
Sbjct 136 EGDQVRLDFADGTHTVADIVIGADGIHSKIREELLGAEAPNYSGWVAHRALIRGVNLAQH 195
Query 183 LEDAELAGEVWGHGKRLG-FIQISPREMYVYATLKVRREEPEDEEGFVTPQRLAAHYADF 241
+ E + W + + + R+ Y + T E D +G A F
Sbjct 196 ADVFEPCVKWWSEDRHMMVYYTTGKRDEYYFVTGVPH--EAWDFQGAYVDSSQEEMRAAF 253

Query 242 DGIGASIARLIPSATTLVHNDLEELAGAS-WCRGRVVLIGDAAHAMTPNLGQGAAMALED 300
+G ++ +LI + ++ L W RGR+V++GDA H M P++ QGA MA+ED
Sbjct 254 EGYHPTVQKLIDATESITKWPLRNRNPLPLWSRGRLVMLGDACHPMKPHMAQGACMAIED 313

pchA

EIEPPJPH_01553 Aminodeoxychorismate synthase component 1

Length=447

Score = 100 bits (249), Expect = 1e-23, Method: Compositional matrix adjust.

Identities = 79/276 (29%), Positives = 128/276 (46%), Gaps = 12/276 (4%)

Query 196 ASALERRQWEAKVSDAVSSVRQGRFGKVVLA-RTQARPLGDIEPWQVIEHLR----LQHA 250
A L+ Q++A ++ G ++ L R +A GD PW+ + LR +
Sbjct 177 AGDLQPEQYKAAFDQVQRYIQAGDCYQINLTQRFRAPCQGD--PWRAYQALRKVCPTPFS 234
Query 251 DAQLFACRRGNACFLGASPERLVRIRAGEALTHALAGTIARGGDAQEDARLGQALLDSAK 310
Q A + L SPER +R+ G+ T + GT R D EDAR + LL S K
Sbjct 235 GYQQLA---DGSALLSFSPERFIRVSEGQVETRPIKGTRPRASDPGEDARNAEELLRSPK 291
Query 311 DRHEHQLVVEAIRTALEPFSE--ALEIPDAPGLKRLARVQHLNTPIRARLADAGGILRLL 368
DR E+ ++V+ +R L E ++++P+ L+ V HL + + +LA L L+
Sbjct 292 DRSENLMIVDLLRNDLGRSCEIGSVKVPELFSLESYPNVHHLVSSVTGQLASDKDALDLI 351

Query 369 QALHPTPAVGGYPRSAALDYIRQHEGMDRGWYAAPLGWLDGEGNGDFLVALRSALLTPGR 428
P ++ G P+ A+ I + E R Y L ++D G D +A+RS L+ G+
Sbjct 352 GDSFPGGSITGAPKIRAMQIIDELEPARRALYCGSLLYVDVRGEMDSSIAIRSLLVKNGQ 411
Query 429 GYLFAGCGLVGDSEPAHEYRETCLKLSAMRDALSAI 464
+ G +V DSE EY E+ K+ + L +
Sbjct 412 VSCWGGGAVVADSEWQAEYEESIAKVRVLMQTLQGL 447

pchB

EIEPPJPH_01863 Isochorismate pyruvate lyase

Length=98

Score = 48.9 bits (115), Expect = 1e-09, Method: Compositional matrix adjust.

Identities = 29/93 (31%), Positives = 45/93 (48%), Gaps = 0/93 (0%)

Query 7 CTGLADIREAIDQIDLDIVQALGRRMDYVKAASRFKANEAAIPAPERVAAMLPERARWAE 66
CT + D+R ID ID ++V L +R V A+ FK + AP RV ++ + AE
Sbjct 5 CTSIEDVRARIDHIDQNLVALLAQRGQLVAQAAAFKKTTDDVRAPARVEQVIAKVRGVAE 64
Query 67 ENGLDAPFVEGLFAQIIHWYIAEQIKYWRQTRG 99
E G VE ++ +I +I E++ G
Sbjct 65 ETGASPEVVERVYRAMIAVFIDEELSVHASLAG 97

Acknowledgment

I would like to express my sincere gratitude to Bioresource Engineering laboratory professors, Prof. Eiichiro Fukusaki, Assoc. Prof. Shuichi Shimma, and Assoc. Prof. Sastia Prama Putri. Their valuable insights and constructive suggestions have guided me plenty throughout my master and doctoral study. I am also grateful to my co-supervisors Prof. Toshiya Muranaka and Prof. Kohsuke Honda for the kind and helpful suggestions to improve my thesis.

I would like to address all of the staff and lab members in Fukusaki Lab. A special thanks to Moke for his helpful assistance and knowledge sharing regarding the genome sequencing. I also wish to thank the MSI team members, especially Takeo-san, Wisman, and Ikuta-san, for being not just a lab mate but also a friend. I could not forget my dear lab members, especially Kadar, Moke, Safira, Fitri, Della, and Mercy. And also my Thai friends, Kik, Arm, Kim, New, Natsu, New, Alps, Keon, and Tua. Thank you for always being by my side. Finally, I would like to thank my family in Thailand for their support, encouragement, understanding, and patience. My gratitude cannot be expressed in words